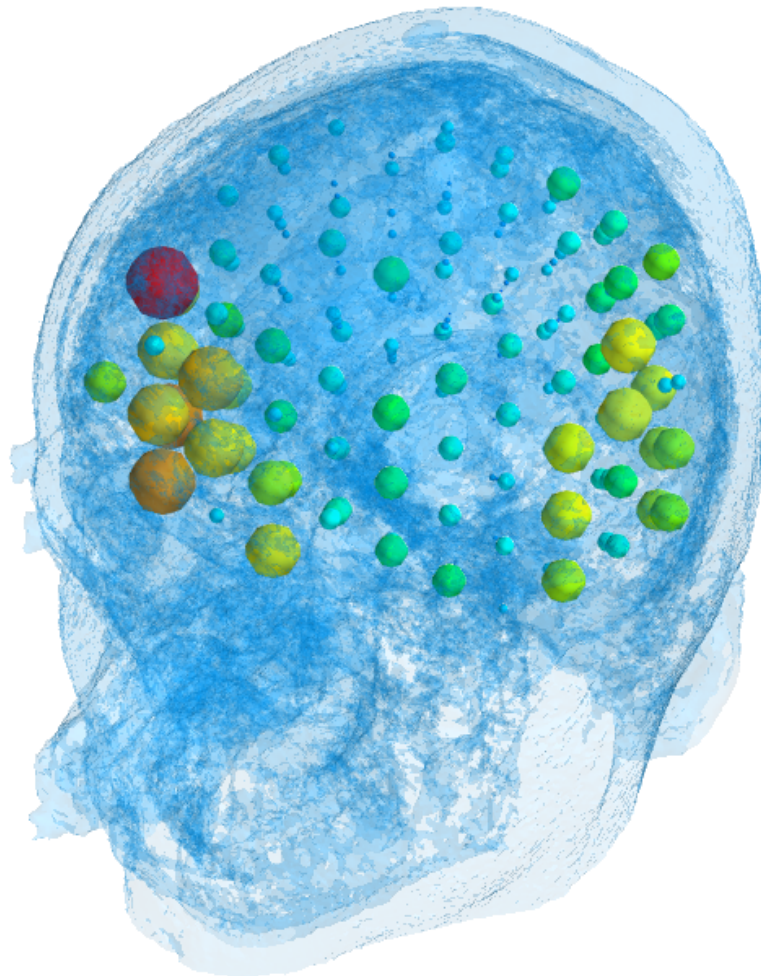




CHALMERS
UNIVERSITY OF TECHNOLOGY



Implementation of the swLORETA in a Cloud Based Service for EEG Analysis

VIGNESH NANDAGOPAL

DEPARTMENT OF ELECTRICAL ENGINEERING
CHALMERS UNIVERSITY OF TECHNOLOGY
Gothenburg, Sweden 2021
www.chalmers.se

MASTER'S THESIS 2021

Implementation of the swLORETA in a cloud based service for EEG Analysis

Vignesh Nandagopal



CHALMERS
UNIVERSITY OF TECHNOLOGY

Department of Electrical Engineering
Biomedical Engineering
CHALMERS UNIVERSITY OF TECHNOLOGY
Gothenburg, Sweden 2021

Implementation of the swLORETA in a cloud based service for EEG Analysis
Vignesh Nandagopal

© Vignesh Nandagopal, 2021.

Supervisor: Ralf Hauße, eemagine Medical Imaging Solutions GmbH
Examiner: Fredrik Brännström, Communication Systems, Electrical Engineering

Master's Thesis 2021
Department of Electrical Engineering
Division of Signals and System
Chalmers University of Technology
SE-412 96 Gothenburg
Telephone +46 31 772 1000

Cover: Source localization using the swLORETA algorithm in a three head dimensional model. The points indicate positions within the brain that have been activated.

Typeset in L^AT_EX
Gothenburg, Sweden 2021

Implementation of the swLORETA in a cloud based service for EEG Analysis

Vignesh Nandagopal
Department of Electrical Engineering
Chalmers University of Technology

Abstract

Electroencephalography is a diagnostic technique that records the brain's spontaneous electrical activity. Once the recording is received, source localization is performed, which facilitates identifying the key areas of the brain responsible for the signal. The issue with electroencephalography is that the instrument takes up a lot of room and the analysis segments are desktop cpu intensive tasks. In this thesis, we investigate at how contemporary cloud computing solutions can be used to build swLORETA, a source localization technique. The electroencephalography becomes more robust with the fundamental deployment of a cloud computing setup with a microservice architecture. The source localization approach produces identical findings to the traditional desktop machine arrangement and visualized in a magnetic resonance image. This configuration opens the way for more appealing electroencephalography and other healthcare-related diagnostic solutions in the future.

Keywords: EEG, source localization, swLORETA, cloud computing

Acknowledgements

First and foremost, I'd like to thank Yibo Wu, my thesis advisor, and Fredrik Brännström, the examiner from Chalmers University of Technology's Electrical Engineering Department. They have always been willing to assist me with any questions I had about my thesis. I'd want to express my gratitude to the Chalmers University of Technology for providing the high-quality education they promised.

I would like to express my heartfelt gratitude to Ralf Hauffe and Frank Zanow of eemagine Medical Imaging Solutions GmbH for entrusting me with this opportunity. I'd also like to thank Jacob Kanev for his unwavering support throughout our thesis discussions, as well as for his advice and insight.

I'd also like to thank my parents, who have been a rock of support throughout this challenging time.

Vignesh Nandagopal, Gothenburg, June 2021

Contents

List of Figures	xi
List of Abbreviations	xiii
1 Introduction	1
1.1 Purpose and Goal	2
1.2 Research Questions	2
1.3 Limitation	2
1.4 Related Work	3
2 Theory	5
2.1 What is EEG?	5
2.1.1 EEG Signals in the Human Body	5
2.2 Characteristics of EEG signals	7
2.3 Acquiring EEG signals	8
2.3.1 EEG Setup	10
2.3.2 Noise and Factors Affecting to EEG Signal	11
2.3.3 Mathematical Representation of EEG	12
2.4 Magnetic Resonance Imaging	12
2.5 EEG Forward Model	13
2.5.1 Dipoles	15
2.5.2 Algebraic Formulation	16
2.6 EEG Inverse Model	17
2.6.1 Generalized Cross Validation	19
2.6.2 sLORETA	19
2.7 Singular Value Decomposition	20
2.7.1 swLORETA	20
2.8 Head Models and Leadfield Matrix	21
3 Methods	23
3.1 swLORETA Algorithm	23
3.2 Cloud Computing	23
3.3 Setup Proposed	25
3.3.1 The Cloud Setup	25
3.3.2 Algorithm in the Cloud	26
3.3.3 Setting up the Solution	27
3.4 Leadfield Matrix	27

3.5	Solution Visualization	28
3.6	Datasets	28
4	Results	29
4.1	Solution Architecture	29
4.1.1	Working of the Solution	29
4.2	Performance	30
4.2.1	Performance of Cloud Setup	30
4.2.2	Comparison between Cloud and Desktop	31
4.3	Solution Visualization	32
4.4	Future Possibilities	36
5	Conclusion	39
	Bibliography	41

List of Figures

2.1	A simple illustration a multiple channel EEG collecting data using electrodes from multiple locations across the scalp of a human being. The image has been modified from [10]. CC BY-NC-ND 2.0	6
2.2	An illustration of a neuron which is the basic building block of the brain [15]. CC BY-SA 4.0.	7
2.3	An illustration of the different brain waves and a description of what activities would be associated with these brain waves. CC0 1.0.	8
2.4	Example of a single channel EEG recording which represents the differential amplification between active and reference electrode. The voltage is on the y-axis and time is in the x-axis.	9
2.5	An illustration of the 10-20 electrode positioning standard followed for EEG. This image has been Released to Public Domain.	10
2.6	A simple circuit diagram explaining the EEG setup similar.	11
2.7	An example of an MRI of the head section. This image is a T1-weighted MRI scan. The following are the basic orientation terms, a coronal plane from the front which is seen on the top left, a sagittal plane that is seen from the side which is in the bottom left and transverse plane observed from the top down which is seen on the right side of the image.	13
2.8	An illustration of the forward model which means calculating the EEG electrode potentials from knowing the values of distribution of current source density in the brain. The left side of the image shows the activation maps of the brain, while the right side shows a schematic of the head with EEG electrodes shown as black dots and their potential values. The image has been modified from [30]. CC BY-SA 3.0.	14
2.9	An example of the EEG inverse model where the current source density, that is induced by dipoles that are spread across the brain is estimated using the EEG electrode potentials. The left side of the image shows the activation maps of the brain, while the right side shows a schematic of the head with EEG electrodes shown as black dots and their potential values. The image has been modified from [30]. CC BY-SA 3.0.	17

3.1	An example of monolithic architecture where all services are combined into one setup is depicted on the left and a microservice architecture for cloud computing which has a separate container performing individual operations is depicted on the right side.	24
3.2	An example of the how the cloud is used is EEG source analysis.	25
3.3	swLORETA Algorithm that has been implemented in the cloud.	26
4.1	The software architecture used in setting up the cloud computing solution of swLORETA. The architecture used follows a microservice architecture.	30
4.2	The performance time of the source localization method using the cloud application tested with the 64 Channel EEG setup.	31
4.3	The performance time of the source localization method using the cloud application tested with the 32 and 20 Channel EEG setup.	32
4.4	A comparison between the time taken for the source localization results using the swLORETA algorithm in the desktop machine and cloud setup is compared.	33
4.5	The swLORETA result that has been overlaid on MRI scan for a 64 Channel Montage. The arrows in the image point towards the activation maps in the brain. The blue activation maps express minimal intensity, fluorescent to yellow symbolises a moderate amount of activity, and red maps designate the maximum intensity of current density. The yellow dot indicates the nasion point of the head, and the red dot indicates the left ear, and the green dot indicates the right ear, respectively. These points are used for reference to read the MRI concerning how the head is oriented.	34
4.6	The swLORETA result that has been overlaid on MRI scan for a 32 Channel Montage. The arrows in the image point towards the activation maps in the brain. The blue activation maps express minimal intensity, fluorescent to yellow symbolises a moderate amount of activity, and red maps designate the maximum intensity of current density. The yellow dot indicates the nasion point of the head, and the red dot indicates the left ear, and the green dot indicates the right ear, respectively. These points are used for reference to read the MRI concerning how the head is oriented.	35
4.7	The swLORETA result has been overlaid on an MRI scan for a 20 Channel Montage. The arrows in the image point towards the activation maps in the brain. The blue activation maps indicate minimal intensity, fluorescent to yellow indicates a moderate amount of activity and red maps indicate maximum intensity of current density. The yellow dot indicates the nasion point of the head, the green dot indicates the left ear and the green dot indicates the right ear respectively. These points are used for reference to read the MRI with respect to how the head is oriented.	36

List of Abbreviations

EEG	Electroencephalography
swLORETA	standardized weighted Low Resolution Tomography
sLORETA	standardized Low Resolution Tomography
SVD	singular value decomposition
MRI	Magnetic resonance imaging
AP	action potential
PSP	postsynaptic potential
GCV	Generalized Cross Validation
ECD	Equivalent Current Dipole
PAN	PreAuricular and Nasion
DICOM	Digital Imaging and Communications in Medicine

1

Introduction

Since the invention of the microprocessor, modern technology has moved towards more compact technologies. Computers, mobile phones, and televisions have benefitted from such changes and have become portable. This trend has now spread to the medical field. The size of devices has reduced dramatically in recent years, while the computational capacity of all of these devices has improved while keeping a compact footprint [1]. These adjustments have also begun to benefit the Electroencephalography (EEG). Recording of the spontaneous electrical activity of the brain is called EEG. EEG systems with higher channel capacity take up more space. However, amplifiers used in EEGs have reduced to a very compact size in recent years [2].

In general EEG systems are connected to a desktop computer which provides a visual stimulus at regular time intervals while recording the signals. Thereby leading the old EEG setup to occupy a larger space [2]. With the upcoming improvements in handheld smartphone devices, it is possible to connect an EEG with a smartphone and start EEG recordings, thereby creating a possibility of shrinking the entire setup. The following stage is to observe and analyze EEG recording utilizing Web applications and cloud-based services that can be accessed from anyplace and eliminate the requirement for a high-powered desktop computer. Such advancements benefit the overall medical diagnostics structure. The ability to conduct EEG recordings at home will become increasingly common in the future. The more these types of setups there are, the easier it is to do an EEG recording. The cloud computing technique allows for faster machine learning-based observations on EEG data as well.

This thesis focuses on analyzing these EEG signals in a cloud-based service, especially on source localization. Source localization of active sources in the brain through EEG signals is a method of brain imaging utilized in a diversity of applications such as investigation of localized epilepsy and attention-deficit/hyperactivity disorder [3].

The thesis is done in collaboration with eemagine Medical Imaging Solutions. They provide complete end to end solutions for medical diagnostics by integrating different modalities such as EEG, Magnetic resonance imaging (MRI), transcranial magnetic stimulation and near-infrared spectroscopy.

1.1 Purpose and Goal

The original plan for the thesis was to use machine learning or deep learning to do source localization. Machine learning algorithms require massive volumes of data. The problem with EEG recordings is that publicly available datasets are low in number, and specifics on the visual stimulus utilized are not provided. The product's overall goal is to make large databanks available for EEG recordings in the future, which can use machine learning or deep learning algorithms.

The goal of this thesis is to implement source localization in a cloud-based framework using the standardized weighted Low Resolution Tomography (swLORETA) algorithm. The technique will visualize the source localization in an averaged MRI image using 20, 32, and 64 channel EEG measurements. The implementation of the thesis work is done in C# programming language. The algorithm is deployed in the cloud using the Docker framework to containerize the implementation. The cloud application will provide the values of source localization when invoked, and a visualization of this is done on an MRI. The solution presented utilizes a basic program that is connected to the internet. It selects the EEG recording, invokes the cloud setup, and the visualization of the EEG occurs. The source localization solution is not an accurate representation of a person's ideal source localization because we are using an averaged MRI for our calculation purposes.

The goals of the master thesis is to :

- Study about EEG and their usage.
- Study about the various inverse solutions used in EEG.
- Study the swLORETA algorithm and implement the algorithm.
- Implement the source localization algorithm within a cloud framework
- Visualise the algorithm and how it works with various EEG channels.

1.2 Research Questions

With the mentioned purpose and goals it is important to formulate a few research questions to answer through the results of thesis. The questions would be the following,

- How to implement the algorithm swLORETA?
- How does the algorithm work as a cloud service and what is the architecture we can use ?
- What are the differences in the solution when using it in a standalone system in comparison with a cloud service?

1.3 Limitation

The implemented solution of source localization is essentially analytical. When attempting to reproduce the swLORETA algorithm, numerous assumptions are made

when attempting to reproduce this algorithm. The method cannot be utilized primarily for direct surgical treatments, which would require individual MRI segmentation [4]. It should be noted that EEG recordings have a low signal-to-noise ratio, and where noise can come from a variety of sources, which could be a problem when analyzing such solutions [5].

Furthermore, it is up to the company to maximize reliability and integrate the project into future applications. When incorporating such features into its products, the organization would devote additional time to product development. Companies work hard to meet product milestones, and such features are likely to appear in future product releases.

1.4 Related Work

Considerable research has been done in the past with regards to source localization algorithms. EEG source localization algorithms are mainly divided into two sections, the parametric and non-parametric approach [6, 7]. Ernesto Palmero-Soler *et al.* [7] proposed the swLORETA algorithm. The swLORETA algorithm's overall resolution is improved by building on the previous standardized Low Resolution Tomography (sLORETA) technique by introducing a singular value decomposition-based lead field weighting method [7, 8]. As a result, the swLORETA method outperforms the sLORETA algorithm in the presence of noise.

The fundamental disadvantage of the source localization approach is that it is computationally expensive due to the inversion of large matrices. Basic desktop configurations may take longer than expected to finish the computations and present the results. This issue can be addressed by implementing the cloud computing technology presented in the thesis. This cloud-based EEG service would be the first of its kind in the health industry. This could pave the way for future medical tests that are more cost effective. This innovation can be seen very soon available in the medical field. If the implementation is successful in products, more analysis tools can be configured in the cloud.

2

Theory

2.1 What is EEG?

An EEG is a recording of the flow of neuronal ionic currents through a pair of electrodes positioned within or on the exterior of the scalp. The intracranial EEG (iEEG) is acquired inside the scalp and is for surgical planning. Specifically, throughout this thesis, the term “EEG” refers to an EEG recorded noninvasively with a combination of electrodes attached to the scalp surface [9].

In the below Figure 2.1, an EEG recording is illustrated. A multiple channel EEG is used and the recorded signal can be seen on the left side of the illustration. EEG recordings is the one of the most efficient techniques to study the electrical activity of the brain [11]. Within fractions of a second after a stimulus is applied, complex patterns of brain activity can be recorded. When compared to an MRI and positron emission tomography, EEG has inferior spatial resolution [12]. Thus, EEG pictures are frequently coupled with MRI scans for better allocation within the brain. The relative intensity and location of electrical activity in various brain areas may be determined using EEG.

Generally, EEG is used in health care to [12]

- Detect awareness, coma, and brain death.
- Determining regions of damage caused by a seizures, head injury, stroke, tumor, etc.
- Overall assessment of the cognitive activity.
- Regulate the depth of anaesthesia.
- Drugs are tested for violent effects.
- Detect sleep problems and physiology.

A simple EEG system incorporates EEG electrodes with conductive material or electrolytic paste, an amplifier comprising filters, an analog to digital converter coupled to a recording device, which is currently a desktop computer system, and a monitor for visualizing the EEG recorded [12].

2.1.1 EEG Signals in the Human Body

The human brain is considered the most complex organ in the body. The brain can be divided into the frontal, occipital, temporal, and parietal lobes. The four lobes have various places and roles that support the human body’s responses and behaviours [13].

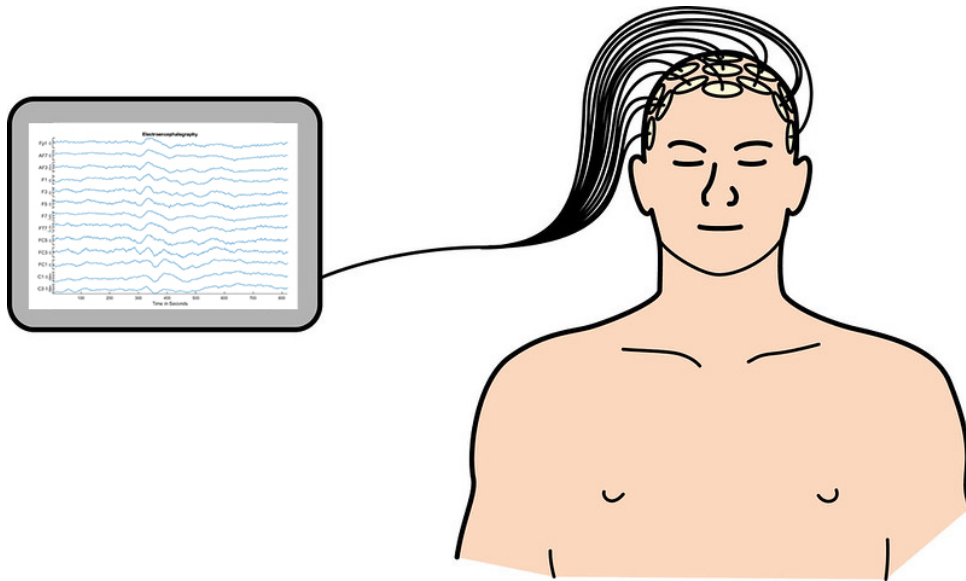


Figure 2.1: A simple illustration a multiple channel EEG collecting data using electrodes from multiple locations across the scalp of a human being. The image has been modified from [10]. CC BY-NC-ND 2.0

Neurons are the basic building blocks of the brain and nervous system. They are the cells responsible for accumulating sensory information from the outside world, transmitting motor instructions to our muscles, and processing and relaying electrical impulses [14]. In Figure 2.2 an illustration of a neuron can be seen. The cell nucleus is the heart of the neuron, relaying instructions to the cell. The axon is a long, thin part of the neuron that binds its nucleus to the dendrite of another [11]. The dendrite is a tiny component of the neuron that contains numerous receptor sites for neurotransmitters provided by an axon terminal. Dendrites can grow on either one or both ends of the cell.

An action potential (AP) is a mechanism in which an ion pumps along the exterior of an axon, rapidly alters its ionic composition and allows an electrical signal to pass immediately down the axon to the next dendrite [16]. As a result of this instant transition in ionic charge, a voltage is produced on both the inside and outside of the neuron's cell membrane [17, 18]. These neurons produce chemicals known as neurotransmitters.

Neuronal electrical activity may be classified into two categories: AP and postsynaptic potential (PSP). If the PSP exceeds the postsynaptic neuron's threshold conduction level, the neuron fires and an AP is launched [11]. The EEG is assumed to be produced predominantly by cortical pyramidal neurons in the cerebral cortex that are aligned perpendicular to the brain's surface. The EEG that is detected is the sum of excitatory and inhibitory PSP from significantly large groups of neurons firing in a synchronized manner [19].

The PSP is unidirectional and is modeled as an equivalent current dipole. These PSPs are primary currents that cause extracellular currents to travel to the furthest reaches of the human body. The movement of these secondary currents via the scalp

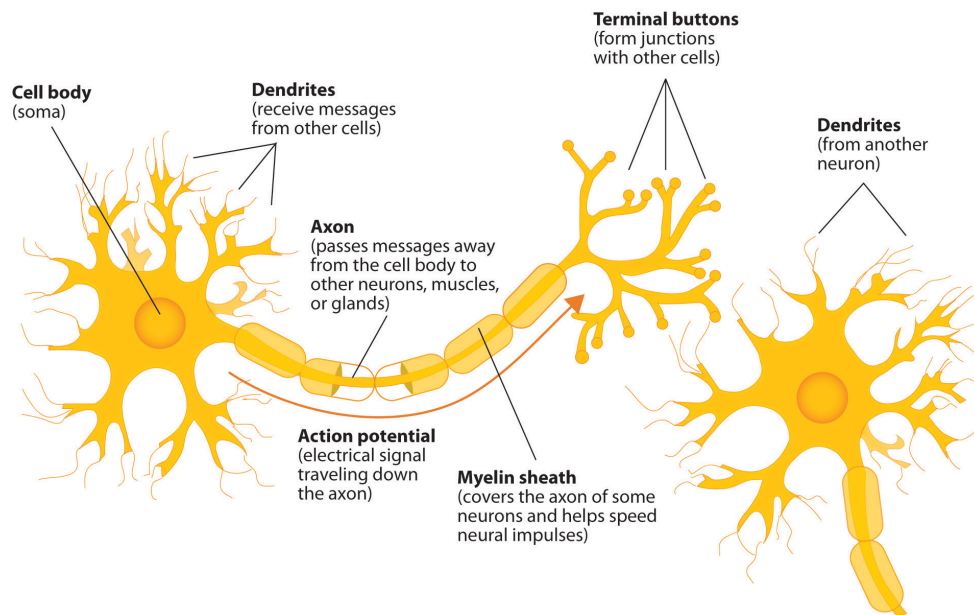


Figure 2.2: An illustration of a neuron which is the basic building block of the brain [15]. CC BY-SA 4.0.

generates a potential difference between two distant places over time, which results in the EEG signal [20].

2.2 Characteristics of EEG signals

One of the most critical elements for evaluating abnormalities in clinical EEGs and interpreting functional behaviors in cognitive research is frequency which is defined as the number of cycles per second. Human EEG potentials are characterized as aperiodic unpredictable oscillations with irregular bouts of oscillations, having billions of oscillating communities of neurons as its source [11]. When healthy individuals shift between states, such as alertness and sleep, the amplitudes and frequencies of such signals change.

EEG signals have a frequency range of 0.01 Hz to approximately 100 Hz, which are separated into five frequency bands. They are categorized as delta (δ), theta (θ), alpha (α), beta (β) and gamma (γ) waves [21]. An illustration of these waves can be seen in Figure 2.3. The delta wave has a frequency range up to 4 Hz, is characterized by the largest amplitudes varying between $100\mu\text{V}$ to $200\mu\text{V}$ and has the slowest wave speed. Deep sleep, major brain illnesses, and waking state are all linked to it. The theta wave has a frequency of 4 to 8 Hz and amplitude between $50\mu\text{V}$ to $100\mu\text{V}$ [11]. Emotional tension, particularly dissatisfaction or disappointment, creative inspiration, as well as a profound meditation, all trigger theta. The alpha wave has a frequency range between 8 to 13 Hz with a $30\text{--}50\mu\text{V}$ amplitude, and it is predominantly found in the brain's posterior parts. The alphas waves are best captured when the patient's eyes are closed or when they are calm. It is frequently

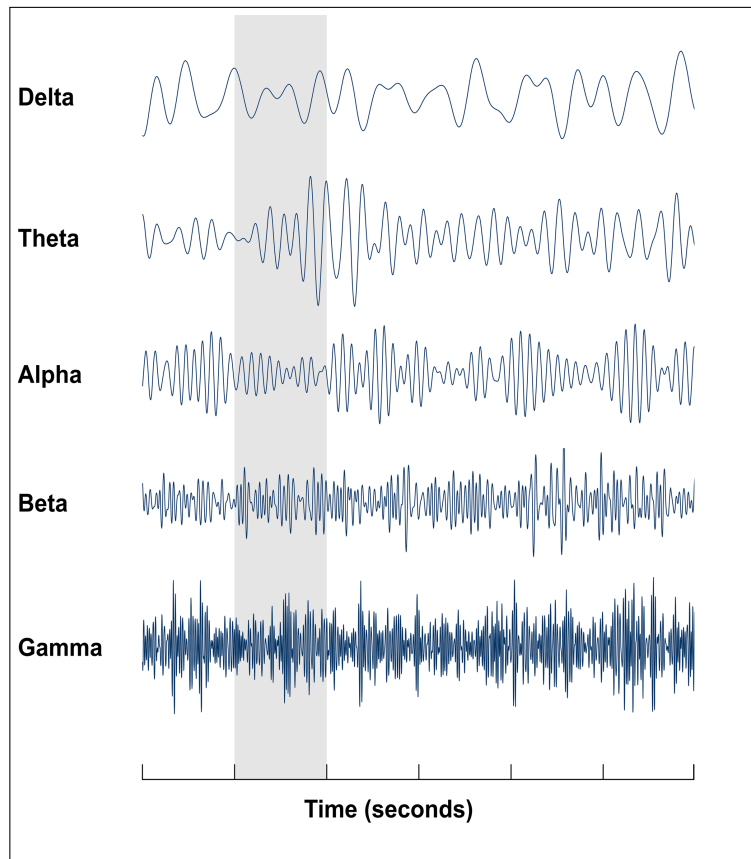


Figure 2.3: An illustration of the different brain waves and a description of what activities would be associated with these brain waves. CC0 1.0.

linked to high levels of mental activity, stress, and tension. The beta wave oscillates between 13 to 30 Hz. It emerges uniformly on both sides in the frontal region, with a small amplitude and fluctuating frequency.

Beta waves are produced when the brain is stimulated and actively engaged in mental activity [11]. These waves indicate higher levels of engagement in the mind. The beta wave is a type of brain wave that is connected with performing activities, paying attention, and focusing on critical challenges. The frequency of gamma waves ranges from 30 Hz and upwards. The maximum frequency of this rhythm is frequently described as being approximately 80 or 100 Hz. It's linked to a variety of cognitive and motor processes. Beyond these frequencies if anything appears these can indicate the onset of epileptic seizures.

2.3 Acquiring EEG signals

Voltages are graphed vertically and time is graphed horizontally in a typical EEG display, producing a near real-time display of ongoing cerebral activity. EEG employs the theory of differential amplification, or recording voltage changes between distinct locations with a pair of electrodes that compare one active exploring electrode site with another nearby or distant electrode [19]. This other electrode is

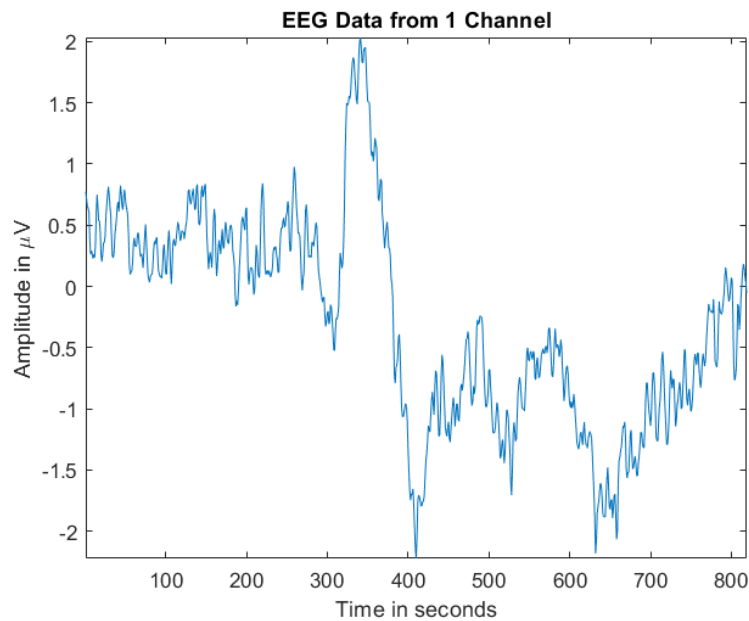


Figure 2.4: Example of a single channel EEG recording which represents the differential amplification between active and reference electrode. The voltage is on the y-axis and time is in the x-axis.

mostly referred to as the reference electrode. EEG waveforms can only be formed by monitoring changes in electrical potential. When the active exploring electrode is much more negative than the reference electrode, the EEG potential vector is directed above the horizontal meridian, but when the reverse is true, the EEG potential vector is directed below the horizontal meridian. EEG channels refer to the signal obtained from differential amplification between the active electrode and the reference electrode [22]. In the Figure 2.4 an example of single channel EEG recording can be seen.

Electrodes are always the first item utilized in bio-signal recordings to transform biopotential signal generated by biopotential sources into electrical signals. EEG electrodes are normally manufactured of metal and come in cup-shaped, disc-shaped, needle-shaped, or microelectrode configurations to monitor intracortical potentials. The majority of scalp electrodes are constructed of non-polarizable materials and are from 1mm to 10 mm in diameter. For most neurophysiologic applications, silver chloride (AgCl) is chosen [23]. An electrolytic paste is applied between the skin and the electrode. The electrical resistance of the skin and the contact between the skin and the electrolytic paste determine the electrode impedance. Noise artifacts can be caused by electrode impedances larger than 5,000 Ohms [24].

Sodium Chloride must be present in large amounts in the electrolytic paste. Throughout the recording, excellent contact between the electrode, conducting paste, and skin should be maintained [9]. EEG recording methods are classified into two types: bipolar and unipolar approaches [9]. The bipolar approach pairs all of the electrodes and records the potential differences between each pair of electrodes. The potential differences between each electrode and a reference electrode are measured

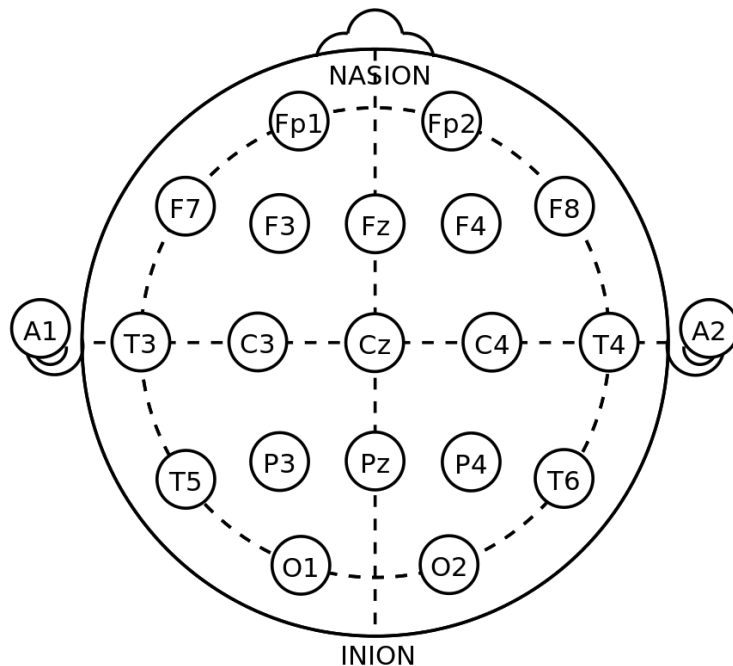


Figure 2.5: An illustration of the 10-20 electrode positioning standard followed for EEG. This image has been Released to Public Domain.

using the unipolar (or monopolar) approach. The reference electrode in the unipolar approach can technically be located anywhere; however, because the dispersion of potential difference on the scalp surface changes depending on the place of the reference electrode, average reference is commonly utilized.

2.3.1 EEG Setup

According to the international federation of clinical neurophysiology (IFCN) guidelines, scalp electrodes are put in conventional places. The IFCN standard array is an adaptation of the “international 10–20 system” [24]. From Figure 2.5 the 10-20 electrode positionings can be seen. It makes use of fixed anatomical features of the skull such as the nasion (the point between the brow and nose) and inion (the hump at the rear of the skull), as well as the pre-auricular point. Distances among skull landmarks (nasion to inion; left pre-auricular to right pre-auricular) are measured, and electrodes are positioned at 10% or 20% of the total distances across them. The 10-20 system gives a maximum of 21 channel EEG. The electrode locations have standardized names that are made up of two symbols [24]. The first symbol is a letter abbreviation of the underlying brain section, while the second is a number denoting its exact location within that region. Fp (frontal-polar), F (frontal), C (central sulcus), P (parietal), O (occipital), and T (temporal) are the abbreviations. Fz, Cz, and Pz are sagittal (midline) electrodes that are in the central line of the scalp. Even-numbered electrodes are on the right side of the skull, whereas odd-numbered electrodes are on the left. Lower-numbered electrodes are closer to the midline, while higher-numbered electrodes are further away.

Montage is a phrase used to describe the layout of EEG electrodes during a recording.

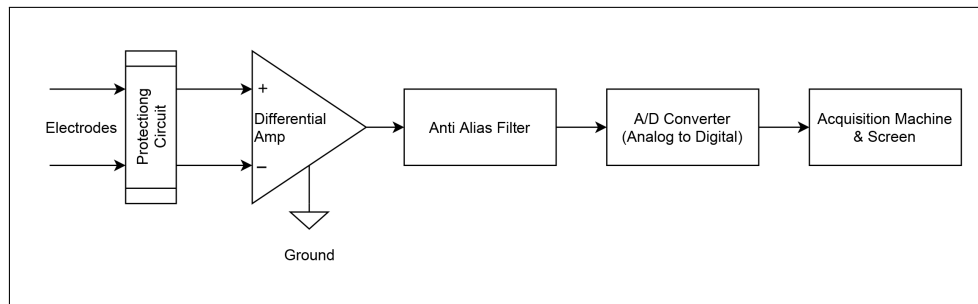


Figure 2.6: A simple circuit diagram explaining the EEG setup similar.

Another typical form of montage is the 10-10 system, which may provide up to 81 channels. The 10-5 technique is followed by a greater density EEG recording with roughly 300 channels. [25].

From Figure 2.6 the fundamental EEG setup can be seen. The electric signals acquired by the EEG electrodes are supplied into an amplifier with multiple channels, for each active electrode on the scalp. The isolation transformer or protection circuit assures that current passes only from the patient to the machine, thus shielding the patient from electric shocks induced by the EEG device. As stated earlier, the active and reference electrodes are sent into the differential amplifier for producing differential voltage. The differential amplifiers must ensure the common mode rejection ratio is high to maintain good performance. After the amplifier the signal is passed to an anti alias filter and then to an analog to digital converter [24].

2.3.2 Noise and Factors Affecting to EEG Signal

Before amplification, the dynamic ranges of the EEG signals are typically $\pm 100 \mu\text{V}$. When these signals traverse through various tissues, they pick up a variety of noise. The noise's properties influence the value and form of the EEG signals. They are divided into the following types [26]

- **Inherent noise:** Noise generated by the electronic equipment combines with the recorded EEG signal. High-quality electrical components can be used to reduce this noise.
- **Ambient noise:** Radiation from electromagnetic equipment is the primary cause of ambient noise. The amplitudes of the ambient noise is considerably larger than those of the EEG signal. This form of noise should be eliminated by usage of a shielded room.
- **Motion artifacts:** When these distortions overlap with the EEG signal, the information signal becomes skewed and erratic. Motion artifacts can be caused by a variety of factors, including (a) electrode interface, (b) electrode cable, (c) ocular artifacts, (d) swallowing, (e) sweating, and (f) breathing. Motion artifacts may be eliminated by designing the electrical circuitry correctly and employing a clever algorithm that isolates and eliminates these artifacts from the EEG signal.
- **Inherent signal instability:** The amplitude of the EEG signal is naturally unpredictable due to inherent signal instability. Electrical signals from the heart

create artifacts influencing the surface potential surrounding the scalp. These artifacts in the EEG data should be suppressed by intelligent systems [26].

2.3.3 Mathematical Representation of EEG

Denote the recorded EEG data at time t and channel m as $x_m(t)$, the collected EEG data matrix $\mathbf{X}(t)$ can be expressed as

$$\mathbf{X}(t) = [x_1(t), \dots, x_m(t)]^T, \quad (2.1)$$

where T denotes the matrix transposition. Each row of $\mathbf{X}(t)$ represents the EEG data recorded at various electrodes at a specific time. Each column of $\mathbf{X}(t)$ represents fluctuations in the signals from a one channel at multiple time points [26].

EEG epoching is a technique for extracting discrete time frames from a continuous EEG data. These time intervals are known as “epochs”, and they are normally time-locked with regard to an event, which is often a form of stimulus.

2.4 Magnetic Resonance Imaging

MRI is an imaging technology that generates comprehensive three-dimensional scans by using the magnetic characteristics of tissue present within the body [27, 28]. The MRI machine creates pictures by employing a combination of high magnetic field strength, magnetic field gradients, and radio waves.

During the MRI scan, the hydrogen proton, present in abundance in water and fat, is utilised to assess the body’s signals. The hydrogen proton revolves along its axis and features the north and south pole, which enables it to function as a magnet [28]. Protons typically spin in the body with their axes randomly regulated. Strong magnets are utilised in MRI machines to produce a magnetic field, which influences the axes of the hydrogen protons to regulate with the magnetic field, resulting in a magnetic vector along the MRI scanner’s axis [27].

In addition, radiofrequency current pulses tailored to the hydrogen proton and the magnitude of the magnetic field are delivered to the patient. The radio waves cause the protons to lose equilibrium and spin, propel them against the magnetic field [27]. When the radio frequency source is switched off, the protons realign with the magnetic field, following the emission of a radio wave signal. The cross-sectional pictures are created by graphing the signal intensity on a greyscale. The magnetic characteristics of the tissue conclude the amount of energy liberated as the protons realign as well as the relaxation duration.

The time it takes for the protons to fully relax may be assessed in two ways. The time taken for the magnetic vector to return to its resting state is one method, known as T1 relaxation. T2 relaxation on the other hand, includes monitoring the time it takes for the axial spin to return to its resting condition. An example of an MRI image is given below in Figure 2.7 of the head section.



Figure 2.7: An example of an MRI of the head section. This image is a T1-weighted MRI scan. The following are the basic orientation terms, a coronal plane from the front which is seen on the top left, a sagittal plane that is seen from the side which is in the bottom left and transverse plane observed from the top down which is seen on the right side of the image.

2.5 EEG Forward Model

Before source localization, it is important to understand the necessity of the EEG forward problem since the same approximations and considerations are used for the EEG inverse model. The EEG forward model is the process of calculating the EEG electrode potentials when knowing values of the current source density [29]. The Figure 2.8 illustrates an example of the forward model.

For the frequency range of the signals recorded in the EEG, no charge can accumulate in the conducting extracellular volume. The active electric source activates all of the fields at the same time [29]. As a result, there are no time delay effects produced. At each occasion, all fields and currents behave as if they were stationary. These are also known as quasi-static conditions. They are not static since brain activity fluctuates throughout time. However, the changes are sluggish in comparison to the propagation effects.

Poisson's equation describes the link between potentials at each and every point in a volume conductor and their applied current sources [29]. A vector field J with

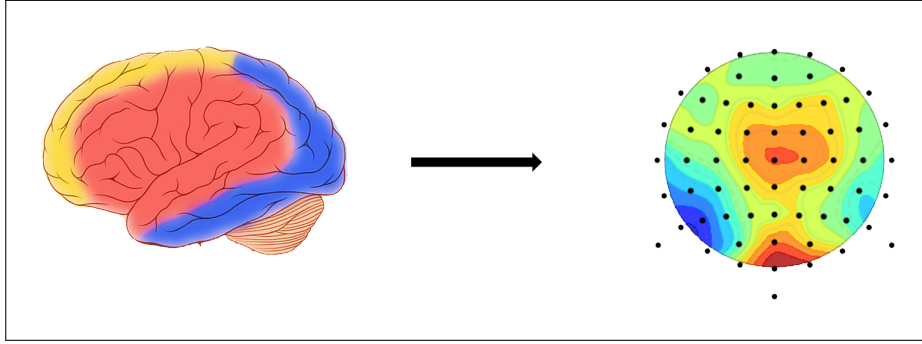


Figure 2.8: An illustration of the forward model which means calculating the EEG electrode potentials from knowing the values of distribution of current source density in the brain. The left side of the image shows the activation maps of the brain, while the right side shows a schematic of the head with EEG electrodes shown as black dots and their potential values. The image has been modified from [30]. CC BY-SA 3.0.

3 dimensional points on the volume of (x, y, z) is defined by,

$$\nabla J = I_m = \lim_{G \rightarrow 0} \oint_{\partial G} J ds, \quad (2.2)$$

where ∇ is the divergence operator. When using the divergence operator, notions such as current source and current sink are utilized [29]. J is the current density vector and is measured in Ampere per meter square (A/m^2). G represents the volume of the conductor and ds is the surface of the volume. The integral of a closed surface through ∂G denotes a flux or current. The unit of ∇J is A/m^3 and is typically referred to as the current source density, which is denoted by I_m . When a net current exits the volume G , this integral is positive and when a net current approaches the volume G , it is negative.

Consider a small volume in the extracellular space that envelops a current source and a current sink, a small volume around the current source at a three-dimensional point r_2 with the following positions (x_2, y_2, z_2) , and a volume surrounded by a current sink with location at a three-dimensional point with the following positions $r_1(x_1, y_1, z_1)$ [29]. (2.2) can be rewritten as,

$$\nabla J = I\delta(r - r_2) - I\delta(r - r_1) \quad (2.3)$$

where I is the current magnitude in Ampere. Using ohm's law one can describe the link between current density J and electric field E with [29],

$$J = \sigma E \quad (2.4)$$

where $\sigma \in \mathbb{R}^{3 \times 3}$ is the location dependent conductivity value and uses the units Siemens per meter (S/m) [29]. The human brain has anisotropic conductivity tissues meaning that conductivity is not uniform in all directions.

The three conductivities in (2.4) symbolise the scalp, the skull and cerebrospinal fluid, which constitute the head model of the human body [29]. Using Poisson's equation, the gradient operator is used to establish a connection between the potential and electric fields which gives,

$$E = -\nabla V \quad (2.5)$$

where the negative sign denotes that the electric field is directed from a high potential area to a low potential area

Substituting (2.5) in (2.4), we can rewrite (2.3) as,

$$\nabla(\sigma\nabla(V)) = -I\delta(r - r_2) + I\delta(r - r_1). \quad (2.6)$$

Considering isotropic conductivities, (2.6) would transform to,

$$\begin{aligned} \frac{\partial}{\partial x} \left(\sigma \frac{\partial V}{\partial x} \right) + \frac{\partial}{\partial y} \left(\sigma \frac{\partial V}{\partial y} \right) + \frac{\partial}{\partial z} \left(\sigma \frac{\partial V}{\partial z} \right) = & -I\delta(x - x_2)\delta(y - y_2)\delta(z - z_2) \\ & + I\delta(x - x_1)\delta(y - y_1)\delta(z - z_1) \end{aligned} \quad (2.7)$$

Similarly we can compute the derivatives for anisotropic conductivities as well. When modelling the forward problem, a few boundary conditions have to be considered [29]. All charge that exits one compartment via the interface must enter the other. All current (charge per second) leaving a compartment with conductivity σ enters the adjoining compartment with a different conductivity σ . The second boundary condition is part of the Dirichlet boundary which states that potentials that cross from one medium to another are constant in value.

2.5.1 Dipoles

When a significant number of neurons are activated at the same time, the electrical activity is significant enough to be detected by the electrodes, resulting in the EEG. A current dipole is considered to be identical to the electrical activity that occurs in the brain [29]. The current source and current sink inject are similar to those of an activated pyramidal neuron at the microscopic level. This model is called the Equivalent Current Dipole (ECD) model.

According to the equivalent current dipole model,

$$\mathbf{d} = Ip\hat{e}, \quad (2.8)$$

where \mathbf{d} is dipole moment and determined by a unit vector \hat{e} (oriented from the current sink to the current source), p denotes the distance separating two monopoles and I is the current magnitude [29].

A dipole is typically split into three dipoles that are aligned along one of the Cartesian axes. The dipoles are positioned in the same spot where the original dipole is. Each of these dipoles has a magnitude equal to the orthogonal projection on the relevant axis which gives us [29],

$$\mathbf{d} = d_x e_x + d_y e_y + d_z e_z, \quad (2.9)$$

where the unit vectors are along the three axes e_x , e_y , and e_z . Moreover, d_x , d_y , and d_z are the dipole components. It's worth noting that Poisson's equation has the property to be scaled linearly. Therefore, a potential V at an arbitrary scalp measuring point r can be divided in two parts due to a dipole at a location r_{dip} and a dipole moment d can be expressed as, [29].

$$V(r, r_{\text{dip}}, \mathbf{d}) = d_x V(r, r_{\text{dip}}, e_x) + d_y V(r, r_{\text{dip}}, e_y) + d_z V(r, r_{\text{dip}}, e_z) \quad (2.10)$$

2.5.2 Algebraic Formulation

In conceptual words, the EEG forward model is to discover the scalp potential $g(r, r_{\text{dip}}, d)$ at an electrode positioned on the scalp at r due to a single dipole with dipole moment d , positioned at r_{dip} in a reasonable amount of time [29]. This entails solving Poisson's equation to determine the potentials $V(r)$ on the scalp for various r_{dip} and d configurations. The electrode potential for several dipole sources can be expressed as

$$V(r) = \sum_i g(r, r_{\text{dip}}, d_i) = \sum_i g(r, r_{\text{dip}}^i, e_d^i) d_i \quad (2.11)$$

The final formulation of the EEG forward model for N electrodes and p dipoles,

$$\begin{aligned} V = \begin{pmatrix} V(r_1) \\ \vdots \\ V(r_{N_s}) \end{pmatrix} &= \begin{pmatrix} g(r_1, r_{\text{dip}}^1, e_{d1}) & \cdots & g(r_1, r_{\text{dip}}^{N_d}, e_{d}^{N_d}) \\ \vdots & \ddots & \vdots \\ g(r_{N_s}, r_{\text{dip}}^1, e_{d1}) & \cdots & g(r_{N_s}, r_{\text{dip}}^{N_d}, e_{d}^{N_d}) \end{pmatrix} \begin{pmatrix} d_1 \\ \vdots \\ d_{N_d} \end{pmatrix} \\ &= G \begin{pmatrix} d_1 \\ \vdots \\ d_{N_d} \end{pmatrix} + \begin{pmatrix} n_1 \\ \vdots \\ n_{N_d} \end{pmatrix}, \end{aligned} \quad (2.12)$$

where $i = 1, \dots, N_d$, $j = 1, \dots, N_s$, $V \in \mathbb{R}^{N_s \times 1}$ is the data measured at the EEG electrodes, $G \in \mathbb{R}^{N_s \times N_d}$ is the Leadfield matrix, $D \in \mathbb{R}^{N_d \times 1}$ is the current source density consisting of all the dipoles at distinct time instants or epochs and $n \in \mathbb{R}^{N_d \times 1}$ is the noise which is generated when recording EEGs [29]. N_s is the number of electrode sensors, and N_d would be number of dipoles. After considering that dipoles have 3 position indexes N_d can be changed to $3N_d$ for our understanding. A more simplified notation of the (2.12) is,

$$V = GD + n. \quad (2.13)$$

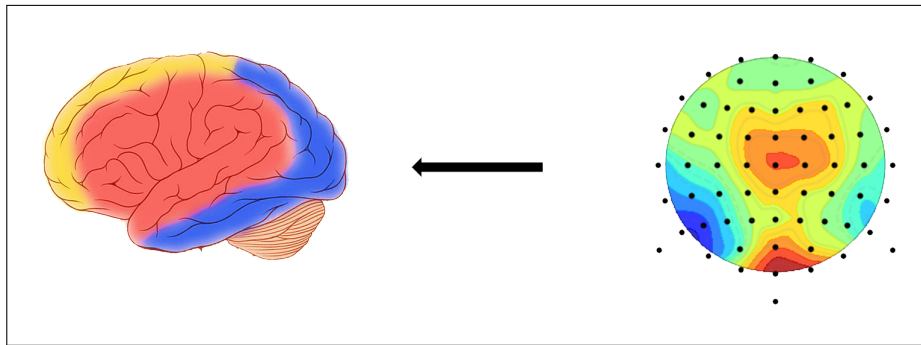


Figure 2.9: An example of the EEG inverse model where the current source density, that is induced by dipoles that are spread across the brain is estimated using the EEG electrode potentials. The left side of the image shows the activation maps of the brain, while the right side shows a schematic of the head with EEG electrodes shown as black dots and their potential values. The image has been modified from [30]. CC BY-SA 3.0.

2.6 EEG Inverse Model

The forward problem determines the scalp potentials that would occur from a current distribution caused by dipoles within the head [6]. The inverse model involves estimating the current source density distribution through the scalp by utilizing the EEG electrode potentials. Figure 2.9 illustrates an example of the inverse model. To formulate an inverse problem in EEG, from (2.13), the current source density D has to be estimated with EEG electrode potentials V at a given epoch. The solution to this model can be tricky since the number of dipoles in the head are comparatively larger in number than the number of EEG electrodes ($3N_d \gg N_s$) [6].

This model is an ill posed problem and a number of considerations can be made to arrive at a solution. Non-parametric and parametric techniques are the two primary approaches to the arriving at the solution for inverse model [6]. Distributed Source Models are another name for non-parametric approaches. Multiple dipole sources with fixed positions and perhaps fixed orientations are dispersed over the whole brain volume or cortical surface in the non-parametric model. The dipoles are considered to be aligned similarly to cortical pyramidal neurons, which are typically orientated to the cortical surface. In the parametric approach only a few dipoles are assumed where their position and direction are uncertain.

In this thesis, the non parametric approach is the main focus and the bayesian framework is best suited to explain the procedure. According to the bayesian framework,

$$\text{posterior} \propto \text{prior} \times \text{likelihood}, \quad (2.14)$$

where prior is any information that is obtained before observing it, likelihood is the information on the possibility of the occurrence of the data and posterior probability is the conditional probability of the data after making observations [31].

In our model, on applying the bayesian framework we get,

$$P(d|V, \lambda, \beta) \propto P(V|d, \lambda)P(d|\beta), \quad (2.15)$$

where a prior distribution $P(d|\beta)$ describes the baseline state of knowledge regarding the mathematical and anatomical attributes of the current density by dipoles D and the likelihood $P(V|d, \lambda)$, which specifies the theoretical model's prediction about the electrode potentials V [32].

By making assumptions about the statistical features of the experimental noise n where,

$$\Sigma_{V,\text{noise}} = \frac{1}{\lambda} \mathbf{I}_{N_s} \quad (2.16)$$

where sensor noise may be described as a multivariate Gaussian distribution with a zero mean [32, 6] and \mathbf{I}_{N_s} is an identity matrix with the dimensions of N_s . According to bayesian statistics the likelihood of the multivariate gaussian distribution is

$$\mathcal{N}(\mu, \Sigma) \propto \exp\left(-\frac{1}{2}(x - \mu)^T \Sigma^{-1} (x - \mu)\right). \quad (2.17)$$

By substituting the inverse model in (2.17) we get [32],

$$P(V|d, \lambda) \propto \exp\left(-\frac{1}{2}(V - GD)^T \Sigma^{-1}_{V,\text{noise}} (V - GD)\right), \quad (2.18)$$

where (2.18) represents the likelihood of our inverse model. Similarly, the prior of our inverse model,

$$\begin{aligned} P(V|d, \lambda) &\propto \exp\left(-\frac{1}{2}D^T \Sigma^{-1} D\right), \\ \Sigma^{-1} &= \frac{1}{\beta} \mathbf{I}_{3N_d}. \end{aligned} \quad (2.19)$$

On substituting (2.18) and (2.19) in (2.15) [32],

$$\begin{aligned} P(d|V, \lambda, \beta) &\propto \exp\left(-\frac{1}{2}[(V - GD)^T \Sigma^{-1}_{V,\text{noise}} (V - GD) + D^T \Sigma^{-1}_D D]\right) \\ &\propto \exp\left(-\frac{1}{2}\lambda \|V - GD\|^2 + \beta \|D\|^2\right). \end{aligned} \quad (2.20)$$

(2.20) is similar to that of tikhnov regularisation [32]. To determine the “best linear unbiased estimate” that maximizes the posterior probability with respect to D , the equation provided by (2.20) is differentiated and equated to zero,

$$D(t) = (G^T G + \alpha \mathbf{I}_{N_s})^{-1} G^T V, \quad (2.21)$$

where (2.21) would be called the *minimum-norm* inverse solution. It is best suited when a problem has an under determined system and when there is a full column rank matrix [32].

$$\alpha = \frac{\lambda}{\beta}, \quad (2.22)$$

where α is the regularization parameter, λ and β are the hyperparameters.

2.6.1 Generalized Cross Validation

The method used to choose the regularization parameter for solving the inverse model in (2.21) is Generalized Cross Validation (GCV) [33, 32]. The objective is to reduce the predicted mean square error as much as possible and the minimal value relates to the ideal value of alpha. The goal of the method is to minimize the mean squared error without knowing the exact value. Due to this, GCV has the ability to reduce signal noise which may not be beneficial [33, 34]. By minimizing the Generalized Cross Validation Error (GCVE) with respect to α and setting it to zero, the value of GCV is obtained. GCVE is defined by

$$\text{GCVE}(\alpha) = \frac{1}{N_s} \sum_{i=1}^{N_s} (V_i - (GD)_i)^2 w_k(\alpha), \quad (2.23)$$

where $w_k(\alpha)$ is defined by

$$w_k(\alpha) = \frac{1 - A_{(k,k)}(\alpha)}{1 - \frac{1}{n} \text{Trace}(A(\alpha))}, \quad (2.24)$$

where $A(\alpha)$ is defined by

$$A(\alpha) = (G^T G + \alpha \mathbf{I}_{3N_g})^{-1} G^T, \quad (2.25)$$

where $(GD)_i$ is the i th vector of the matrix obtained from the product of current source density obtained from (2.21) and the leadfield matrix G .

2.6.2 sLORETA

The problem with respect to minimum-norm inverse solution is that it relies only on sources near the cortical surface and doesn't consider other current source generators deep within the brain [8]. This can be resisted using the sLORETA method. For simplification, (2.21) is modified to,

$$D(t) = (G^T G + \alpha \mathbf{I}_{N_s})^{-1} G^T V = T(\alpha) V. \quad (2.26)$$

The sLORETA approach executes a location-wise inverse weighting of the minimum-norm inverse on the EEG electrode data and leadfield matrix. Then the variance of the solution is calculated and the solution is standardized meaning the solution is divided by its standard deviation. This procedure produces a zero localization error [8]. Statistical parametric maps (SPMs) are produced as a result of this standardization. The equation for the current density covariance estimate

$$\Sigma_{\hat{D}} = T(\alpha) \Sigma_D T(\alpha)^T = K^T (K K^T + \alpha \mathbf{I}_{N_s})^{-1} K. \quad (2.27)$$

Using (2.27), (2.26) can be rewritten as,

$$\hat{D}_{\text{sLORETA}} = \{\Sigma_{\hat{D}}\}^{-\frac{1}{2}} D = \{\Sigma_{\hat{D}}\}^{-\frac{1}{2}} T(\alpha) V. \quad (2.28)$$

(2.28) is the final form for sLORETA. The method of Singular valued decomposition can be used to calculate the sLORETA estimates which speeds up the computation [8, 32].

2.7 Singular Value Decomposition

The singular value decomposition (SVD) for a matrix $A \in \mathbb{R}^{n \times p}$ [34],

$$A = USV^T = \sum_i^n u_i \sigma_i v_i^T. \quad (2.29)$$

where the columns of $U \in \mathbb{R}^{n \times n}$ are the left singular vectors, $S \in \mathbb{R}^{n \times p}$ is a diagonal matrix and contains singular values, and $V^T \in \mathbb{R}^{p \times p}$ has rows that are the right singular vectors [35]. The SVD represents an extension of the original data in a coordinate system with a diagonal covariance matrix. Finding the eigenvalues and eigenvectors of AA^T and $A^T A$ is the first step in calculating the SVD. The columns of V are made up of $A^T A$ eigenvectors, while the columns of U are made up of AA^T eigenvectors. Furthermore, the singular values in S are square roots of AA^T or $A^T A$ eigenvalues are organized in decreasing order.

A SVD has the corresponding properties:

- Both U and V are orthonormal, and thereby when multiplying the vector with its transpose, they produce an identity matrix [35].
 - $U^T U = I$, where I is a $n \times n$ matrix.
 - $V^T V = I$, where I is a $p \times p$ matrix.
- S consists of non-negative singular values on the diagonal, where $\sigma_1 \geq \sigma_2 \geq$

$$\dots \geq \sigma_p, S = \begin{bmatrix} \sigma_1 & 0 & \dots & 0 \\ 0 & \sigma_2 & \dots & 0 \\ \vdots & \vdots & \ddots & 0 \\ 0 & 0 & \dots & \sigma_p \\ 0 & 0 & \dots & 0 \end{bmatrix}$$

2.7.1 swLORETA

In swLORETA, a normalization to account for the sensors' variable sensitivity to current sources at different depths has to be performed. The columns of the leadfield matrix G comprise dipole current sources distributed across the brain. These dipoles have three components at a particular location that are oriented in different directions whose effect is not taken into consideration when formulating the sLORETA solution [32]. As a result, to compensate for this circumstance, a normalization must occur to estimate the relative sensitivity and alter the associated values of G to make the sensitivities equal [32]. The covariance matrix of G needs to be modified to ensure this standardisation occurs. A simple method is to separate Leadfield G into the SVD decomposition as follows

$$D = U_D S_D V_D^T, \quad (2.30)$$

where, when the SVD decomposition of the leadfield matrix produces S_D that consists of 3 diagonal elements whose values correspond to a three-dimensional point in

the head [32]. These values depict the sensitivity of the current dipole at a particular point in the head. From this, we can rewrite the covariance of current source density estimated in (2.28) as,

$$\begin{aligned}\Sigma_D^{\frac{1}{2}} &= S_D^{-\frac{1}{2}} \otimes \mathbf{I}_3, \\ \Sigma_D &= (\Sigma_D^{\frac{1}{2}})^T (\Sigma_D^{\frac{1}{2}}),\end{aligned}\tag{2.31}$$

where \otimes is the kronecker product. Using the standardised leadfield Matrix G , (2.13) consisting of the forward model can be rewritten as,

$$V = (G\Sigma_D^{\frac{1}{2}})(\Sigma_D^{-\frac{1}{2}}D) + n.\tag{2.32}$$

The sLORETA equation 2.28 to find current source density can be rewritten as,

$$D = \Sigma_D^{-\frac{1}{2}} D_{\text{sLORETA}}\tag{2.33}$$

2.8 Head Models and Leadfield Matrix

It is very important for usage of an accurate head model to model our inverse solution. In this thesis, the sphere approximation of the head model will not be used. It is important to remember that the solution that is to be calculated for the inverse model is an analytical solution. A volume conductor model is used in generating an approximate human head model. A volume conductor model can be calculated either by usage of Boundary element method, Finite element method or finite difference method.

The Boundary Element Method (BEM) is focused on integral equations with unknowns at the interfaces, whereas the FDM (finite difference method) or FEM (finite element method) take into account the whole volume [36]. As a result, the BEM dramatically minimizes the quantity of unknowns while also needing just surface meshes rather than volume meshes.

3

Methods

This chapter describes the several approaches used in this thesis work. In this thesis, the swLORETA algorithm is used for source localization. Then a simple program utilizing the algorithm is built followed by deployment in the cloud.

3.1 swLORETA Algorithm

The non-parametric approach was chosen since it replicates the beliefs that we have of the brain's neurophysiological properties. The parametric approach is based on the notion that EEG signals are generated by a limited number of point sources, the location, and orientation of which are undetermined. The non-parametric method is based on the notion that several sources with specific placements are spread throughout the brain. The swLORETA is chosen because it works better in the presence of noise and the algorithm adjusts for the sensors' variable sensitivity to current sources at varying depths [32].

The inverse model of the EEG is an ill-posed problem [6]. The lead field matrix generated has a higher number of columns than rows. This makes it challenging to invert the matrix required to solve the problem. This leads us to use the minimum-norm estimates method. The entire procedure of swLORETA algorithm is computationally expensive. Powerful computers with sophisticated hardware are required to compute the solution quickly. This leads us to using a cloud solution which can highly benefit the solution. Cloud servers have highly sophisticated hardware and are easy to setup with current advancements.

3.2 Cloud Computing

In this section the cloud computing aspect of the thesis is discussed. The cloud is the most important aspect of this thesis.

Cloud computing is the supply of computing services—including servers, storage, databases, networking, software, analytics, and intelligence—via the Internet (“the cloud”) in order to provide quicker development more flexible tools, and efficiencies [37]. Cloud computing serves as a hub for the highest disruptive technologies, notably mobile Internet, knowledge work automation, the Internet of Things (IoT), and big data [38].

The following are the major reasons to use cloud computing in the thesis:

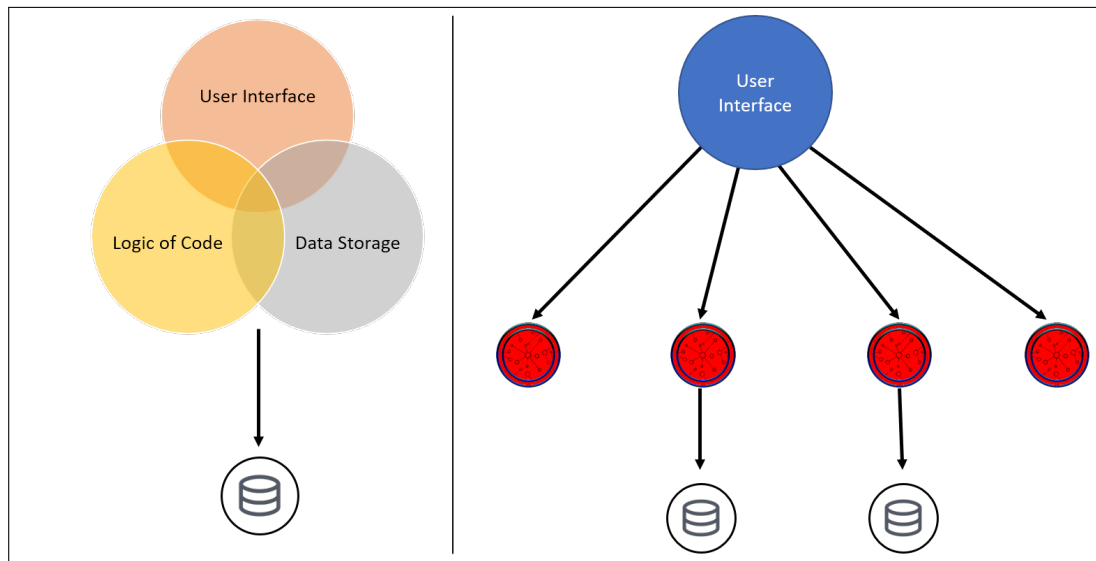


Figure 3.1: An example of monolithic architecture where all services are combined into one setup is depicted on the left and a microservice architecture for cloud computing which has a separate container performing individual operations is depicted on the right side.

- Significant cost savings in hardware and software procurement leading to simplistic arrangements that are more efficient.
- Increased operation agility can be obtained when using the processing power of data centers that generally have high-quality hardware on demand.
- Scalability of the product for future releases.
- Increased productivity in the overall diagnostic setup due to reduced hardware components in healthcare.

Traditionally, applications are created as monolithic pieces of software. Adding new features compels restructuring and updating everything from the application's operations, communications and security [39]. As a result, traditional monolithic applications have extended lifecycles, that are rarely updated, and causes a major impact to the entire application. In addition, this architecture leads to problems of dropping the entire application for future developments. Cloud computing solutions initially followed such architectures as well.

Microservices is a type of cloud architecture developed to combat these issues. Each application is composed of a collection of services, each of which runs in its process and communicates using application programming interface (API) [40]. Below in Figure 3.1 depicts an illustration of microservice architecture in comparison to a monolithic architecture. Microservices have an overall advantage in offering future scalability of the entire service, data is decentralized and isolated failures leads to less downtime. Microservices are present within containers which provide the functionality needed to run the services. Containers contain the required software, libraries, and configuration files for these individual services to run independently. Thus, through containers, a proper interaction occurs over well-defined channels between services.

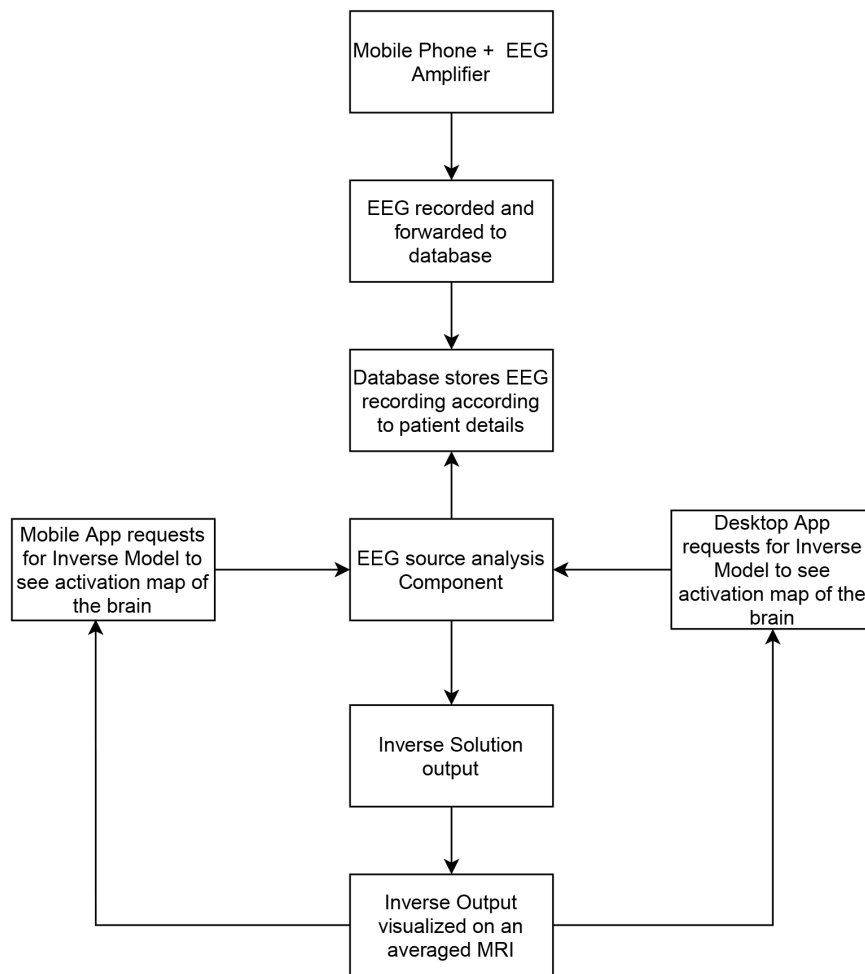


Figure 3.2: An example of the how the cloud is used is EEG source analysis.

3.3 Setup Proposed

The company currently has developed an intelligent tablet-sized amplifier that can record up to a 64-channel EEG. They have also developed a primary application to record an EEG recording and transfer it to the cloud. In the following sections, we propose a cloud setup using the microservice architecture that incorporates the swLORETA algorithm. This setup can take advantage of the existing cloud setups that are present in today’s technological revolution.

3.3.1 The Cloud Setup

The Figure 3.2 illustrates the workflow of the proposed cloud setup. A mobile application connected to an EEG amplifier and EEG electrodes records the EEG signals. Once the recording is done the recorded signals are pushed to a database in the cloud. Another cloud container consists of the EEG source analysis implementation using the swLORETA algorithm. When the source analysis component is called the output produced by the algorithm is pushed back to the application and the source is visualized on an MRI.

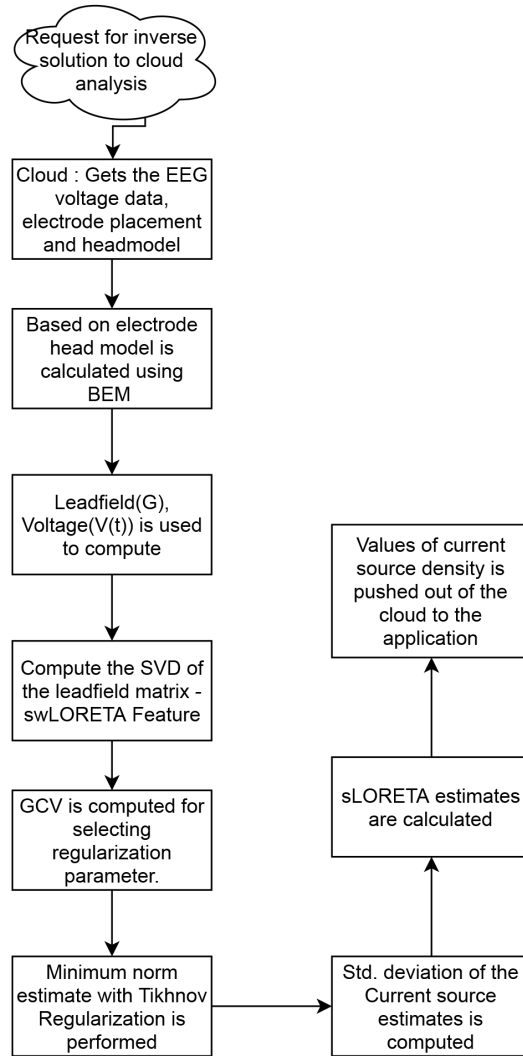


Figure 3.3: swLORETA Algorithm that has been implemented in the cloud.

3.3.2 Algorithm in the Cloud

A simple illustration of the swLORETA algorithm can be seen in Figure 3.3. A few important details are required for computing the algorithm. The value of voltages recorded through the EEG at one time instance and EEG electrode montage.

The algorithm works in the following way, the EEG recording for one time instance and the electrode montage that are selected are transmitted via gRPC to the source analysis cloudserver. The first step would be to get the lead field matrix. The leadfield matrix varies according to the EEG montage as the positions of the electrodes are different for the 20, 32 and 64 channel montage. Once calculated the singular value decomposition of the lead field matrix is done for standardization. Typically the size of the leadfield matrix would be of the size $N_s \times 3N_d$. The EEG recording for one time instance would be a vector of size $N_s \times 1$. The truncated SVD is used to compute the leadfield matrix since the number of columns in the leadfield matrix are excessively huge. The value for Generalized cross validation is calculated and

the minimum norm estimate with tikhnov regularization is performed. Next, the standard deviation is calculated for the current density estimates and the sLORETA estimates are calculated. The calculated values are then pushed back via gRPC to the application for visualization.

3.3.3 Setting up the Solution

This section describes how the complete solution is setup. The entire solution is setup with the guidance of the company eemagine. The programming language C# is used to write the algorithm. Once a rudimentary functioning code was implemented, the algorithm's values are validated against the reference data. After the algorithm passed all of the unit tests, it is exported to the cloud server as an individual service to the container. All build prerequisites are exported as an executable application. Docker is a software that assists in building containers with all their required dependencies and export microservices as an image to a cloud server. With the help of docker, our program is containerized and deployed to a cloud server.

An API framework is a communication protocol, and it is required for the services to communicate between one another and external applications outside the cloud server. In our application, we use gRPC. gRPC is a remote procedure call that facilitates seamless communication between client and server applications and makes it easier to create connected systems. It is a very lightweight communication protocol and is very useful for the internet of things communication pattern.

3.4 Leadfield Matrix

The boundary element method is used in generating the head model required to produce the leadfield matrix. The boundary element method produces triangular meshes of around a reconstructed surface of the T1 weighted MRI image. The central point of these triangular meshes is a node. BEM solves the system of integral equations over a closed surface and a uniform conductivity is taken for a single component. There are 3 components that need to be modelled which are the brain, scalp and cerebrospinal fluid.

In this thesis, the BEM calculations for the head model are not done. A headmodel has already been constructed using BEM and the nodes of these triangles are stored in a file. The leadfield is calculated separately using the file of the headmodel and stored in a separate file for the 20, 32 and 64 channel EEG montage. The leadfield matrix is a three-dimensional matrix which is stored in the cloud. In the future, the leadfield calculations for other type of EEG montages will be done. Currently, EEG caps or nets that are commonly utilized have fixed spatial arrangement and remain constant.

3.5 Solution Visualization

The cloud analysis setup pushed out the values of current source density after the calculations based on the respective montage. Once the values have been got, the values have to be mapped on to an averaged MRI image for the user to see. This section explains the process.

The MRI images are in Digital Imaging and Communications in Medicine (DICOM) and have their own respective coordinate system. The output from the swLORETA algorithm is in a PreAuricular and Nasion (PAN) coordinate system. The values of MRI have to be transformed into the PAN system so that the values of the current source density can be mapped on to the brain. This is possible because the MRI is rearranged to form a 3D image that can be picture as a collection of a 3 dimensional matrix. The output of the cloud is also in 3 dimensional space. It is only necessary to overlay these results on the MRI to generate a result. A rotation matrix needs to be generated for to convert the MRI to the PAN System.

3.6 Datasets

The dataset for the EEG reading is of a patient whose details is not known. The EEG analog signal is recorded for 32 and 64 scalp locations, accordingly, using the A.N.T. amplifier with a gain of 30000 and 64 Ag-AgCl electrodes installed on a WaveGuard cap which follows the 10-5 electrode systems. The EEG signals are recorded at a 512 Hz sampling rate using a 0.01 to 200 Hz bandpass filter. In total, two recordings are used to formulate the results. Furthermore, any residual artifacts over $\pm 75 \mu V$ in any channel are discarded. Finally, epochs are created using artifact-free data.

4

Results

In this part, the results will be shown. In Section 4.1, the solution architecture and setup is discussed. In Section 4.2, the performance of the cloud solution for determining the results is determined. In Section 4.3, the results of the visualization in the MRI is discussed, and in Section 4.4, the possibilities that can occur with the incorporation of this setup is discussed.

4.1 Solution Architecture

The software architecture is depicted in Figure 4.1. The proposed architecture is a microservice architecture. Two services are deployed and operating on the cloud server. The first service is used to receive and store EEG recordings made using a smartphone. The recordings are kept on a SQL server that is not part of the cloud container but rather on a separate server. This is done to ensure that if the cloud container begins to malfunction, it may be restarted without impacting patient data.

The source analysis service, which employs the swLORETA algorithm, is the second service. To pick an existing EEG recording in the cloud, a simple client-side application has been constructed. This service is deployed in a separate docker container as well. The client-side program is currently running on a desktop computer. It is a very rudimentary setup. The values selected on the desktop application are examined on the cloud, and the results are returned. Both services are decoupled in nature. Only one service would be unavailable if one of the services failed or needed to be upgraded. This is the primary benefit of the microservice architecture.

The client-side application and the source analysis application are developed using C#. Using Docker, both the services are containerized with their software dependencies. The communication protocol gRPC is used for transmitting information across these applications and within the cloud for accessing information.

4.1.1 Working of the Solution

When the client-side application is opened, the gRPC protocol on the client application is connected to the cloud container server. The gRPC protocol on the server side pushes the information of the EEG data files stored in the database. The client-side application would display the selected EEG that is present within the cloud. Next, a user can select the EEG recording and the EEG epoch they wish to perform

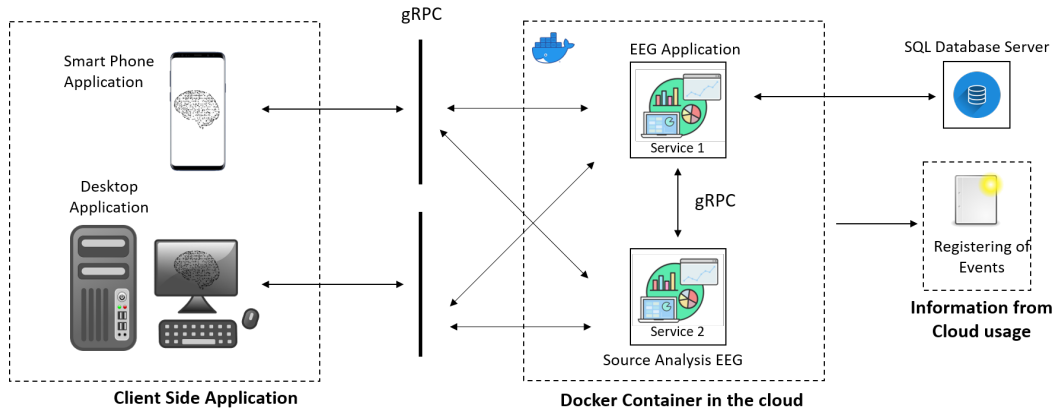


Figure 4.1: The software architecture used in setting up the cloud computing solution of swLORETA. The architecture used follows a microservice architecture.

the source localization analysis on. The gRPC protocol in the client pushes the values of the EEG voltages at a particular epoch or timestamp to the source analysis service within the cloud container. Through internal gRPC communication, the source analysis service gets the values and performs the analysis. Then the values of the current source density from the source analysis service is pushed back by the gRPC server protocol to the application from which the initial communication was sent. The visualization using the MRI takes place in the client-side application, and the results can be seen below.

4.2 Performance

In the following section we will investigate the performance of the cloud setup first and then conduct another experiment to compare it to an application that is totally setup on the desktop without any cloud computing.

4.2.1 Performance of Cloud Setup

The experimental setup uses a rudimentary client application. The 64, 32 and 20 Channel EEG recordings are used to test the performance of the application. The 64 channel EEG source localization is more computationally expensive than the 32 and 20 channel EEG setups. In Figure 4.2 the performance of the cloud setup can be seen. The grid spacing used in the boundary element method for generating the mesh was 20mm in length. This produces 200 dipoles across the head, which have three-dimensional positions in the headspace. The grid spacing can be decreased to achieve a more accurate result. The more the spacing is reduced, the more computationally intensive is the process.

A series of 10 simulations using different time stamps/epochs of the 64 Channel EEG recording are done to measure the time taken for the cloud solution. On average 48.04 seconds was the time taken for the solution to be displayed on the client side application.

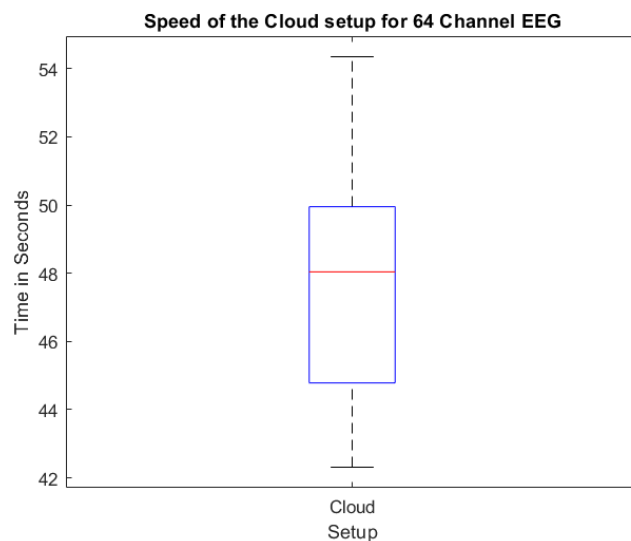


Figure 4.2: The performance time of the source localization method using the cloud application tested with the 64 Channel EEG setup.

Similarly, 10 simulations using different time stamps/epochs of the 32 and 20 Channel EEG recordings are done to measure the time taken for the cloud solution. The average time taken to arrive at the solution for the 32 Channel EEG setup was 26.1 seconds and the average time taken for the 20 Channel EEG setup was 18.8 seconds. The Figure 4.3 contains the performance plots of the 32 and 20 Channel EEG setups.

4.2.2 Comparison between Cloud and Desktop

To conclude whether the cloud setup is beneficial, a basic desktop application containing the implementation of the source localization algorithm is set up without the cloud interface, and an application of the cloud solution is compared. The 64 Channel EEG recording is used. A total of 5 simulations is done at different timestamps in both setups. The grid spacing used in the boundary element method for generating the head mesh is 20mm in length. This produces approximate 200 dipoles across the head, which have three-dimensional positions in the headspace. From Figure 4.4 the speed comparison of both the cloud setup and desktop are compared.

The overall median in the performance of the cloud solution is 48.20 seconds, and the desktop setup is 47.58 seconds. The cloud solution is as fast as the desktop setup. The cloud solution also had one time which was around 39 seconds, and at the same time, the longest time taken was 56 seconds which is relatively slow compared to the desktop setup. The desktop setup had significantly less variation in performance time. It is vital to remember that the computer utilized for the experiment has a lot of processing capacity compared to most hospital desktop configurations.

The speed of the cloud can improve by optimizing the C# code. The entire implementation can be improved with a better cloud interface if the setup is successful when merging with existing products. By allocating more computational power in

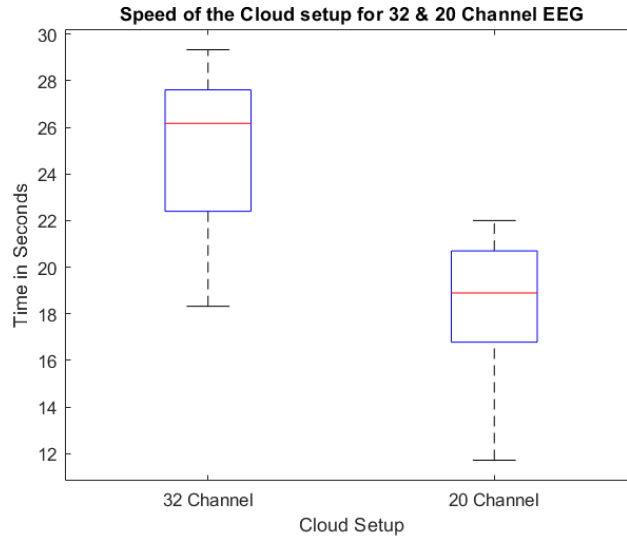


Figure 4.3: The performance time of the source localization method using the cloud application tested with the 32 and 20 Channel EEG setup.

the cloud, the results can be more agile since cloud servers have better access to sophisticated hardware. It is always important to remember that a smooth internet connection is required to ensure the results are transmitted to the cloud and received from the cloud in a fast manner.

4.3 Solution Visualization

Two EEG recordings are used for the 20, 32 and 64 channel EEG montages. The 20 and 32 channel EEG montage use the same recording since the 20 channel has the same locations and only additional locations are present in the 32 channel EEG. The grid spacing used in the boundary element method for generating the head mesh is 20mm in length. This produces approximate 200 dipoles across the head, which have three-dimensional positions in the headspace. This would produce 600 positions of dipoles in a three dimensional axis.

The overall precision recorded with the reference data provided by the company is $1E-10$ for the swLORETA implementation. This means that the algorithm is ideally replicating the swLORETA algorithm.

From Figure 4.5 the result from the swLORETA algorithm that would be displayed on the client side application is visible for a 64 channel EEG montage.

The leadfield matrix is of the size 64×600 . The EEG values are a vector of 64×1 and the current source density is a 600×1 vector. The resulting vector of current source density is a three-dimensional vector that has been collapsed into a two-dimensional vector to speed up the computation. The MRI was a $256 \times 256 \times 186$ matrix and the result obtained from the swLORETA algorithm is converted to the MRI coordinate system. The same MRI has been used for the following results as well. The three dots of the colours red, green and yellow on the MRI indicate the position of the

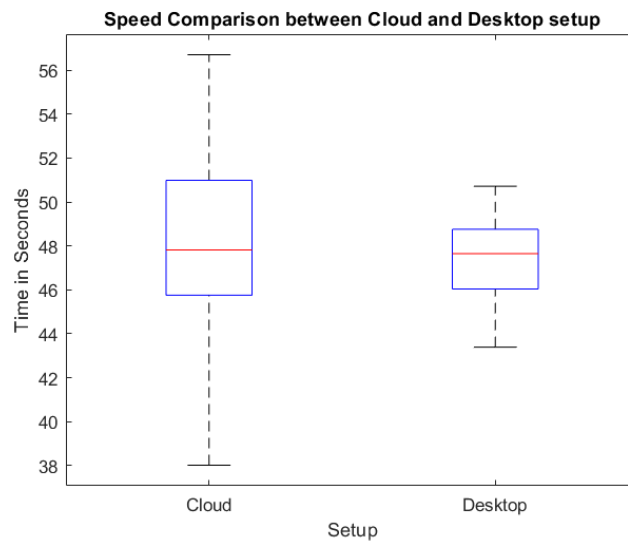


Figure 4.4: A comparison between the time taken for the source localization results using the swLORETA algorithm in the desktop machine and cloud setup is compared.

nasion (central point on the head), the left ear and right ear in each of the planes of the MRI.

From Figure 4.5 the arrows point towards the location of the activity in the brain. The regions that have been colored are the activation maps in the brain and the color map used indicates that blue has the least intensity, yellow has a medium intensity and red has the highest intensity. This color scheme remains the same for the other results produced as well. Only if the algorithm works is when these color maps can be produced. The intensity maps follow a cubic spline interpolation to map the area around them to show the activation area in the brain.

In the given Figure 4.6 the result for the swLORETA algorithm for a 32 channel EEG montage is displayed. The leadfield matrix is of the size 32×600 . The EEG values is a 32×1 vector and the current source density is a 600×1 vector. The colourmap on the MRI Figure 4.6 indicate the activity maps in the brain. The EEG recording used for the 32 channel EEG montage is different in comparison to the 64 channel EEG montage. Similarly the coordinates of the swLORETA algorithm have been transformed to that of the MRI to overlay the results.

In the given Figure 4.7 the result for the swLORETA algorithm for a 20 channel EEG montage is displayed. The leadfield matrix is of the size 20×600 . The EEG values is a 20×1 vector and the current source density is a 600×1 vector. The colourmap on the MRI Figure 4.7 indicate the activity maps in the brain.

From the above results it can be seen that the visualization of the 64 channel EEG montage is significantly better and more clearer when using the cubic spline interpolation since a good amount of values have been generated. The 32 channel and 20 channel EEG montage use the same recording. The 20 channel montage result is not as clear as that of the 32 channel. This may be due to less number of active

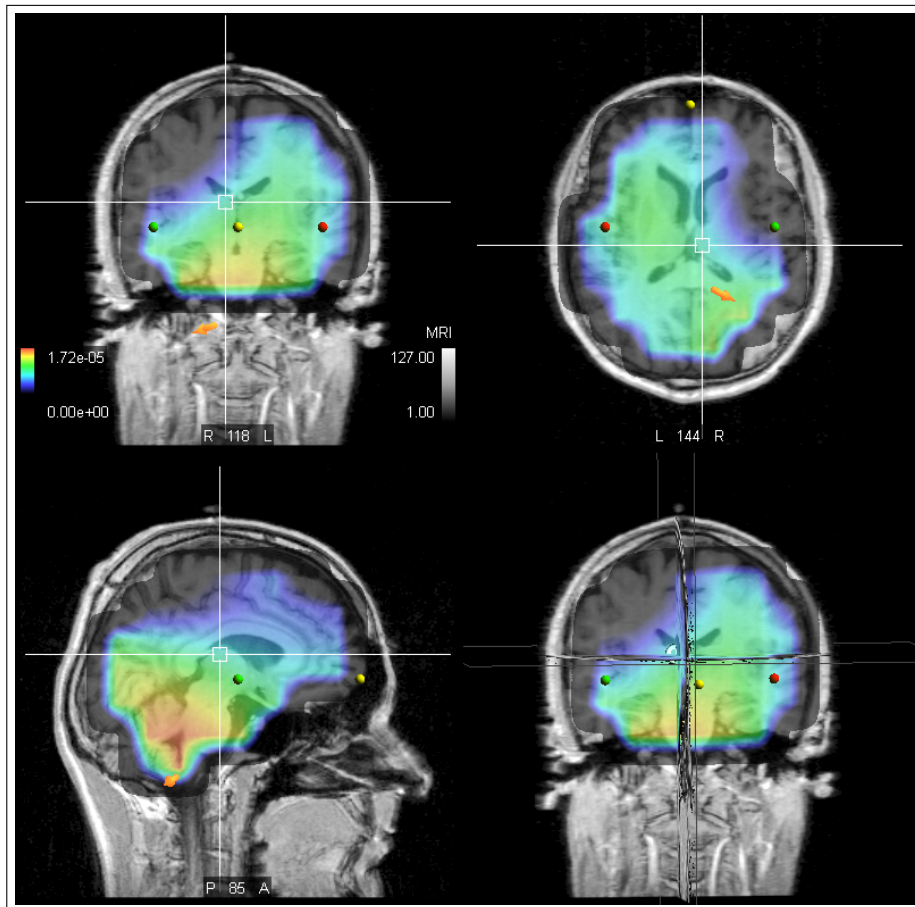


Figure 4.5: The swLORETA result that has been overlaid on MRI scan for a 64 Channel Montage. The arrows in the image point towards the activation maps in the brain. The blue activation maps express minimal intensity, fluorescent to yellow symbolises a moderate amount of activity, and red maps designate the maximum intensity of current density. The yellow dot indicates the nasion point of the head, and the red dot indicates the left ear, and the green dot indicates the right ear, respectively. These points are used for reference to read the MRI concerning how the head is oriented.

electrodes which cause a more poor activity map. From this it can be inferred that the higher density EEG channels produce a more accurate result for activity maps in the brain.

The result of swLORETA algorithm, that is the current source density produced due the 64 Channel EEG montage is in the below matrix. The matrix is 600×1 vector, only a few values are displayed. The numbers have double precision, the numbers here are rounded off.

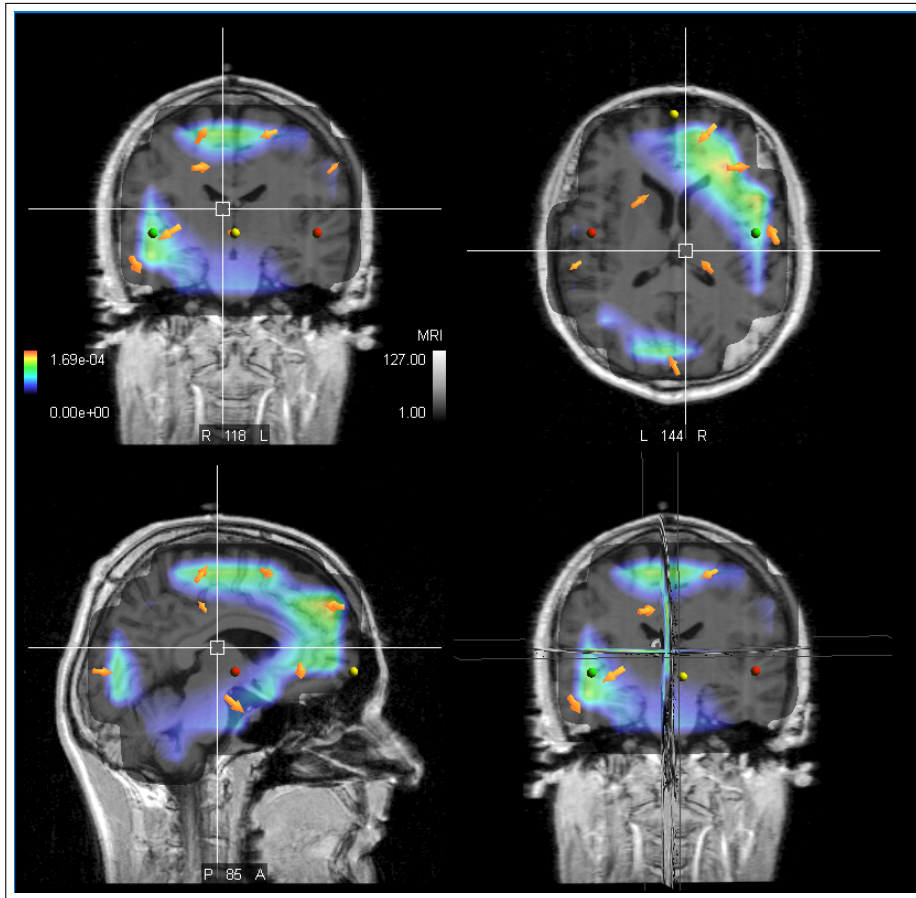


Figure 4.6: The swLORETA result that has been overlaid on MRI scan for a 32 Channel Montage. The arrows in the image point towards the activation maps in the brain. The blue activation maps express minimal intensity, fluorescent to yellow symbolises a moderate amount of activity, and red maps designate the maximum intensity of current density. The yellow dot indicates the nasion point of the head, and the red dot indicates the left ear, and the green dot indicates the right ear, respectively. These points are used for reference to read the MRI concerning how the head is oriented.

$$D = \begin{bmatrix} -0.000761343 \\ -0.00035879 \\ -8.2644e - 05 \\ 2.96053e - 05 \\ 4.94648e - 05 \\ 7.04373e - 05 \\ -0.000710948 \\ -0.000389392 \\ \vdots \\ -0.000808136 \\ -4.0058e - 05 \\ 0.000126475 \\ 0.000249668 \end{bmatrix} \quad (4.1)$$

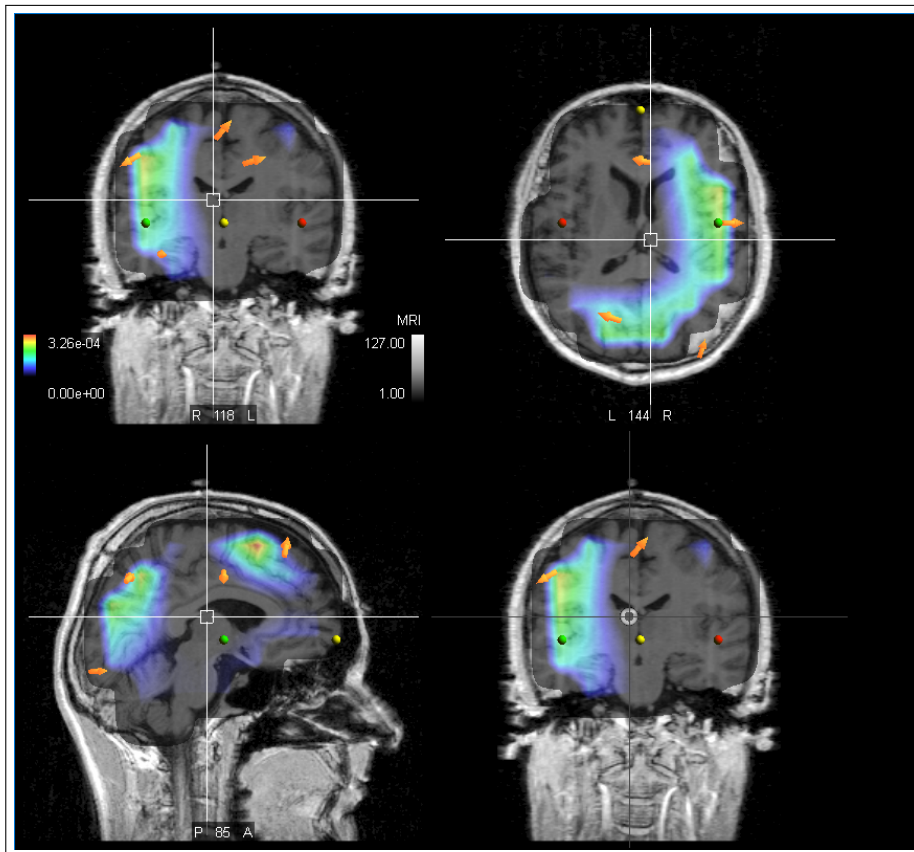


Figure 4.7: The swLORETA result has been overlaid on an MRI scan for a 20 Channel Montage. The arrows in the image point towards the activation maps in the brain. The blue activation maps indicate minimal intensity, fluorescent to yellow indicates a moderate amount of activity and red maps indicate maximum intensity of current density. The yellow dot indicates the nasion point of the head, the green dot indicates the left ear and the green dot indicates the right ear respectively. These points are used for reference to read the MRI with respect to how the head is oriented.

4.4 Future Possibilities

This setup proves to be very beneficial in multiple ways. The EEG amplifier developed for this setup is the size of a handheld smart tablet. Due to the design proposed, anybody can use smart tablets or smartphones to record an EEG. Thereby reduction in the overall EEG setup. The amplifier for the EEG has been made into a very compact design, thereby ensuring ease of portability.

A desktop computer is a critical component of the EEG setup [2]. The recent shortage of microprocessor supplies in the world has caused a shortage in next-generation computers with high computation power. A cloud setup for the EEG is essential to decrease the requirement of compelling computers. With this setup, the requirement for such setups can decrease, and the hospital can benefit from a more low resource cost. The desktop machine might become completely redundant when this setup can be successfully replicated on tablets and smartphones.

Machine learning algorithms are computationally intensive and take up major processing power for classification. By using the cloud solution, a machine learning

service can be deployed in the cloud and can make faster predictions on the data since cloud servers have better access to sophisticated hardware.

The centralized design offered by a database in the cloud provides accessibility of the data worldwide. The advantage is patients can get additional consultations from doctors who are not within their vicinity.

With upcoming developments of dry electrodes coupled with the handheld EEG amplifier and cloud setup, EEG recordings can be done remotely and with minimal supervision, which improves the overall productivity of healthcare workers. The hospital can prepare multiple recordings simultaneously, or patients can do EEG recordings at home as well.

5

Conclusion

The thesis work investigates the performance of the swLORETA source localization algorithm in a cloud-based framework. According to the results in Chapter 4, with the use of a rudimentary application, we can see how well the swLORETA algorithm works. Then the swLORETA algorithm was exported to a cloud-based framework which also had satisfactory results. The application was also able to match the speed of a highly sophisticated desktop computer, but the desktop computer does edge out on overall performance. By optimizing the code further and allocating more computation power in the cloud server, it is possible to improve the speed of the solution. This result makes it a desirable solution to incorporate into existing EEG products to reduce the complexity of the entire EEG setup. Furthermore, various future components can be built and deployed onto the server with minimal downtime by incorporating such a microservice architecture.

When coupling the cloud solution with the mobile EEG setup, the portability of the solution is high. The setup paves the way to a new range of EEG recording products. With such portable EEG devices, better visual stimuli and examinations could be performed. The design of such devices has the potential to translate to other medical products that perform computationally intensive calculations as well. The cost of the EEG setup may be reduced exponentially with such improvements in the overall design. The cost of cloud computing solutions are extraordinarily minimal and only tends to reduce more in the future.

Second, machine learning methods require a significant amount of processing power. The microservice architecture, which employs decoupled applications, can improve the performance of machine learning algorithms. In microservice design, many machine learning and analytical algorithms can be run concurrently and effectively. This expedites the complete process. This is the direction medical devices will take in the future.

Third, the source localization algorithm can be implemented utilizing machine learning or deep learning. This would be far faster than even the existing implementation.

Bibliography

- [1] Steve Furber. “Microprocessors: the engines of the digital age”. In: *Proceedings of the Royal Society A: Mathematical, Physical and Engineering Sciences* 473.2199 (2017), p. 20160893.
- [2] Patrick Ledwidge, Jeremy Foust, and Adam Ramsey. “Recommendations for Developing an EEG Laboratory at a Primarily Undergraduate Institution”. In: *Journal of Undergraduate Neuroscience Education* 17.1 (2018), A10.
- [3] Pablo Andrés Muñoz-Gutiérrez et al. “Localization of active brain sources from EEG signals using empirical mode decomposition: A comparative study”. In: *Frontiers in integrative neuroscience* 12 (2018), p. 55.
- [4] Seppo P Ahlfors and Gregory V Simpson. “Geometrical interpretation of fMRI-guided MEG/EEG inverse estimates”. In: *NeuroImage* 22.1 (2004), pp. 323–332.
- [5] Bin He et al. “Electrophysiological imaging of brain activity and connectivity—challenges and opportunities”. In: *IEEE transactions on biomedical engineering* 58.7 (2011), pp. 1918–1931.
- [6] Roberta Grech et al. “Review on solving the inverse problem in EEG source analysis”. In: *Journal of neuroengineering and rehabilitation* 5.1 (2008), pp. 1–33.
- [7] Ernesto Palmero-Soler et al. “swLORETA: a novel approach to robust source localization and synchronization tomography”. In: *Physics in Medicine & Biology* 52.7 (2007), p. 1783.
- [8] Roberto Domingo Pascual-Marqui et al. “Standardized low-resolution brain electromagnetic tomography (sLORETA): technical details”. In: *Methods Find Exp Clin Pharmacol* 24.Suppl D (2002), pp. 5–12.
- [9] Chang-Hwan Im. *Computational EEG Analysis*. Springer, 2018.
- [10] Wikimedia Commons. *Electrode locations of International 10-20 system for EEG (electroencephalography) recording*. 2010. URL: <https://www.flickr.com/photos/easy-pics/9408344706/in/album-72157634666274830/>.
- [11] Siuly Siuly, Yan Li, and Yanchun Zhang. “Electroencephalogram (EEG) and its background”. In: *EEG Signal Analysis and Classification*. Springer, 2016, pp. 3–21.
- [12] Michal Teplan et al. “Fundamentals of EEG measurement”. In: *Measurement science review* 2.2 (2002), pp. 1–11.
- [13] Priyanka A Abhang, Bharti W Gawali, and Suresh C Mehrotra. *Introduction to EEG-and speech-based emotion recognition*. Academic Press, 2016.
- [14] *What is a neuron?* Aug. 2019. URL: <https://qbi.uq.edu.au/brain/brain-anatomy/what-neuron>.

- [15] Wikimedia Commons. *Components of neuron*. File: Components of neuron.jpg. 2014. URL: https://commons.wikimedia.org/wiki/File:Components_of_neuron.jpg#file.
- [16] Harold L. Atwood and W. A. MacKay. *Essentials of neurophysiology*. B.C. Decker, 1989.
- [17] Neil R Carlson. *Foundations of physiological psychology*. Pearson Education New Zealand, 2005.
- [18] Saeid Sanei and JA Chambers. “Introduction to EEG”. In: *EEG signal processing* (2007), pp. 1–34.
- [19] Jeffrey W Britton et al. “Electroencephalography (EEG): an introductory text and atlas of normal and abnormal findings in adults, children, and infants”. In: (2016).
- [20] Chang-Hwan Im. “Basics of EEG: Generation, Acquisition, and Applications of EEG”. In: *Computational EEG Analysis*. Springer, 2018, pp. 3–11.
- [21] Xiao Jiang, Gui-Bin Bian, and Zean Tian. “Removal of artifacts from EEG signals: a review”. In: *Sensors* 19.5 (2019), p. 987.
- [22] Zohreh Zakeri. “Optimised use of independent component analysis for EEG signal processing”. PhD thesis. University of Birmingham, 2017.
- [23] Ali Bulent Usakli. “Improvement of EEG signal acquisition: An electrical aspect for state of the art of front end”. In: *Computational intelligence and neuroscience 2010* (2010).
- [24] Sándor Beniczky and Donald L Schomer. “Electroencephalography: basic biophysical and technological aspects important for clinical applications”. In: *Epileptic Disorders* 22.6 (2020), pp. 697–715.
- [25] Aamir Saeed Malik and Hafeez Ullah Amin. *Designing EEG experiments for studying the brain: Design code and example datasets*. Academic Press, 2017.
- [26] Mahmoud I Al-Kadi, Mamun Bin Ibne Reaz, and Mohd Alauddin Mohd Ali. “Evolution of electroencephalogram signal analysis techniques during anesthesia”. In: *Sensors* 13.5 (2013), pp. 6605–6635.
- [27] U.S Department of Health and Human Services. *Magnetic Resonance Imaging (MRI)*. [Online; last visited 13-April-2020]. URL: <https://www.nibib.nih.gov/science-education/science-topics/magnetic-resonance-imaging-mri>.
- [28] Abi Berger. “Magnetic resonance imaging”. In: *BMJ* 324 (2002), p. 35. ISSN: 7328. DOI: <https://dx.doi.org/10.1136%2Fbmj.324.7328.35>. URL: <https://www.ncbi.nlm.nih.gov/pmc/articles/PMC1121941/>.
- [29] Hans Hallez et al. “Review on solving the forward problem in EEG source analysis”. In: *Journal of neuroengineering and rehabilitation* 4.1 (2007), pp. 1–29.
- [30] Wikimedia Commons. *Cerebral vascular territories*. File: Cerebral vascular territories.svg. 2010. URL: https://commons.wikimedia.org/wiki/File:Cerebral_vascular_territories.jpg.
- [31] William M Bolstad and James M Curran. *Introduction to Bayesian statistics*. John Wiley & Sons, 2016.
- [32] Ernesto Palmero Soler. “Functional imaging based on swLORETA and phase synchronization”. PhD thesis. 2016.

-
- [33] Gene H Golub, Michael Heath, and Grace Wahba. “Generalized cross-validation as a method for choosing a good ridge parameter”. In: *Technometrics* 21.2 (1979), pp. 215–223.
- [34] Mohammed Jamil Aburidi. “A Comparative Study of the Regularization Parameter Estimation Methods for the EEG Inverse Problem”. PhD thesis. 2016.
- [35] Kirk Baker. “Singular value decomposition tutorial”. In: *The Ohio State University* 24 (2005).
- [36] Geoffray Adde et al. “Symmetric BEM formulation for the M/EEG forward problem”. In: *Biennial International Conference on Information Processing in Medical Imaging*. Springer. 2003, pp. 524–535.
- [37] Microsoft. *What Is Cloud Computing? A Beginner’s Guide: Microsoft Azure*. URL: <https://azure.microsoft.com/en-us/overview/what-is-cloud-computing/>.
- [38] Bhaskar Prasad Rimal and Ian Lumb. *The Rise of Cloud Computing in the Era of Emerging Networked Society*. Ed. by Nick Antonopoulos and Lee Gillam. Cham: Springer International Publishing, 2017, pp. 3–25. ISBN: 978-3-319-54645-2. DOI: 10.1007/978-3-319-54645-2_1. URL: https://doi.org/10.1007/978-3-319-54645-2_1.
- [39] *Why should you use microservices and containers?* URL: <https://developer.ibm.com/depmodels/microservices/articles/why-should-we-use-microservices-and-containers/>.
- [40] NetApp. *What Are Microservices? And How Do They Work?* Jan. 2019. URL: <https://www.netapp.com/knowledge-center/what-are-microservices/#:~:text=Microservices%20are%20an%20architectural%20approach,more%20than%2020%20years%20ago..>

DEPARTMENT OF ELECTRICAL ENGINEERING
CHALMERS UNIVERSITY OF TECHNOLOGY
Gothenburg, Sweden
www.chalmers.se



CHALMERS
UNIVERSITY OF TECHNOLOGY